The influence of 3D canopy structure on modelled photosynthesis

Stretton, M. A. ORCID: https://orcid.org/0000-0002-1444-5735, Quaife, T. ORCID: https://orcid.org/0000-0001-6896-4613, Wilkes, P. and Disney, M. (2025) The influence of 3D canopy structure on modelled photosynthesis. Agricultural and Forest Meteorology, 366. 110437. ISSN 1873-2240 doi: 10.1016/j.agrformet.2025.110437 Available at https://centaur.reading.ac.uk/122006/

Agricultural and Forest Meteorology 366 (2025) 110437

Contents lists available at ScienceDirect

Agricultural and Forest Meteorology

journal homepage: www.elsevier.com/locate/agrformet

The influence of 3D canopy structure on modelled photosynthesis

Megan A. Stretton [a,*], Tristan Quaife [a], Phil Wilkes [b,c,d], Mat Disney [b,c]

[a] National Centre for Earth Observation, Department of Meteorology, University of Reading, Reading RG6 6ET, UK
[b] UCL Dept of Geography, Gower Stret, London, WC1E 6BT, UK
[c] National Centre for Earth Observation, UCL Dept of Geography, Gower Street, London, WC1E 6BT, UK
[d] Royal Botanic Gardens Wakehurst, Selsfield Rd, Haywards Heath, West Sussex, RH17 6TN, UK

ARTICLE INFO

Keywords:
Photosynthesis
Canopy structure
Radiative transfer modelling
DART model
Terrestrial lidar scanning

ABSTRACT

Vegetation is one of the largest terrestrial sinks of atmospheric carbon dioxide, driven by the balance between photosynthesis and respiration. Understanding the processes behind this net flux is critical, as it influences the global atmospheric carbon dioxide concentration and hence climate change. A key factor determining the carbon flux into the land surface is the absorption of light by vegetation, used to drive photosynthesis. However, climate models commonly represent vegetation canopies as homogenous slabs of randomly positioned leaves. By contrast, real forests generally exhibit large amounts of 3-dimensional heterogeneity.

We examine the impact of including measured 3D vegetation canopy structure on modelled gross primary productivity (GPP) by looking at how leaf area is distributed. We introduce a methodology to calculate GPP using output from the explicit Discrete Anisotropic Radiative Transfer (DART) model, following the approach commonly used in land surface schemes. The sensitivity of modelled GPP to canopy structure assumptions in Earth system models is explored, using 3D structural information derived from six forest plots using Terrestrial Lidar Scanning (TLS) data. Here, we use the spatial resolution as a proxy for the canopy structure, with the very coarsest simulations containing no spatial variability in leaf location, with variability introduced as the resolution of the simulations becomes finer. In almost all cases, the simulated GPP is reduced, and with the finest resolution this is up to 25 %. This contrasts with recent studies showing the opposite effect. In the few cases where the GPP increased, this was only marginal (< 2.5 %). These results suggest that not accounting for the impact of 3-dimensional canopy structure could lead to significant biases in land surface models, particularly in forest's contribution to the global carbon budget. We suggest that vegetation structure is considered, explicitly or through a correction factor, alongside a comparison to existing clumping approaches.

1. Introduction

Terrestrial vegetation is one of the largest global sinks of carbon, absorbing ~1/3 of all CO_2 emissions (Friedlingstein et al., 2020) and, in some regions, has the potential to switch to a carbon source with climate change. This terrestrial carbon budget is driven by the balance between the respiration and production, with this net flux varying from a net uptake by the land of ~ 4 PgC $year^{-1}$, to a net emission of carbon of ~0.3 PgC $year^{-1}$ (Le Quéré et al., 2018; Sitch et al., 2008). This net carbon flux influences atmospheric CO_2 concentration and therefore the progress of climate change. The global primary production (GPP) is the process of turning this atmospheric CO_2 into chemical energy, primarily by vegetation through photosynthesis, with the GPP flux estimated at 123 ± 8 Pg C $year^{-1}$ (Ciais et al., 2013). Even small errors in the GPP will lead to uncertainties in the models that are bigger than the net flux. Consequently, understanding the processes that drive GPP, and being able embed this knowledge into Earth system models is a key task for climate science.

Modelling of GPP in both climate and Earth system models has undergone several advances in recent decades. For example, by including the influence of the nitrogen cycle (Kattge et al., 2009; Sokolov et al., 2008; Thornton et al., 2007), and the use of trait-based modelling approaches (Madani et al., 2018; Peaucelle et al., 2019; Rewald et al., 2021; Yan et al., 2023). However, a fundamental aspect of modelling photosynthesis that has changed very little is the assumption that absorption of light by plant canopies – a first order determinant of photosynthesis – is analogous to that of a plane parallel, semi-infinite turbid medium – the so-called turbid medium assumption. This

* Corresponding author.
E-mail address: m.a.stretton@reading.ac.uk (M.A. Stretton).

https://doi.org/10.1016/j.agrformet.2025.110437
Received 13 May 2024; Received in revised form 31 January 2025; Accepted 2 February 2025

implies that leaves are randomly located in space and the top and bottom of the canopy is perfectly flat and parallel with the underlying soil, and that there is no horizontal variability in the vegetation properties. The use of these assumptions stems from the need for computational efficiency within climate modelling. Structurally more explicit radiative transfer schemes that resolve high levels of canopy detail have too heavy computational and data requirements (e.g., Kobayashi and Iwabuchi (2008); Gastellu-Etchegorry et al. (2015)). The turbid medium assumption, however, permits the construction of so-called two-stream models of radiative transfer for vegetation that can be solved analytically (Sellers, 1985) and have been the standard in climate models for several decades.

One of the key advances in modelling canopy light interception that has been adapted in some climate models is the splitting of leaves into sunlit and shaded components (Dickinson et al., 2006; Norman, 1993; Sinclair et al., 1976). This has been shown to have a significant effect on modelled GPP (Sprintsin et al., 2012). This is especially true under the influence of diffuse radiation, such as the work by Mercado et al. (2009) which showed photosynthesis is more efficient during diffuse light (i.e., cloud cover or increased atmospheric aerosols) and found that the global dimming period between 1960–1999 enhanced the land carbon sink by 25 %. However, these studies are still bound within the turbid medium assumption, and hence lack any description of the 3D canopy structure, which impacts model processes (Alton et al., 2006; Pinty et al., 2006).

Loew et al. (2014) showed that not accounting for canopy structure can lead to a significant underestimation of the amount of radiation absorbed by leaves and suggest that this will result in an underestimation of GPP. Some other studies have tried to address the lack of vegetation structure in vegetation canopy models, using simple clumping factors (Kucharik et al., 1999; Nilson, 1971). These factors account for the observed tendency of vegetation to self-organise in 3D at multiple scales (crowns, within-crown, branch level) allowing more effificent absoprtion through the canopy. The use of clumping factors provides a basic way to simulate the impact on radiation absorption by discrete tree crowns, or the clumping of leaves (or needles) around a branch, and means that for a given leaf area index (LAI), more leaves are shaded than sunlit than without clumping. Studies disagree about the impact of clumping on the resultant GPP, with Chen et al., (2012) finding a decrease in GPP by 12.1 PgC $year^{-1}$ globally when incorporating clumping into BEPS (Boreal Ecosystem Productivity Simulator). In contrast, Braghiere et al. (2019) showed an increase of 5.53 $\pm$ 1.02 PgC $year^{-1}$ using the Joint UK Land Environment Simulator (JULES), and Li et al. (2023) showed increased GPP in the shaded canopy of 6.9–8.2 PgC $year^{-1}$ and in the sunlit canopy of 5.9–7.2 PgC $year^{-1}$. Some studies have expanded this work further by exploring whether these clumping indices could be solar zenith angle dependent (Braghiere et al., 2020; Ni-Meister et al., 2010; Pinty et al., 2006).

Interestingly, despite producing varied increases and decreases in GPP, the studies by Chen et al. (2012) and Braghiere et al. (2019) used the same clumping dataset as an input (He et al., 2012), so the differences between them seem to result from the treatment of the radiative transfer. The BEPS model uses a so called big-leaf model, which treats the total amount of absorbed radiation rather than the sunlit and shaded components separately. The version of the Community Land Model (CLM), CLM5, used by Li et al., (2023), assumes a single vegetated layer, but splits the canopy into sunlit and shaded components.

Some newer model developments go a step further, implementing multi-layer representation of the vegetation canopy, which allow variability of properties such as LAI. Examples of these include multi-layer developments for ORCHIDEE, where studies have examined the impact on the energy balance and turbulent fluxes (e.g., Chen et al., (2016); Ryder et al., (2016)), as well as multi-layer developments for CLM, such as CLM-ml (Bonan et al., (2018); Song et al., (2021)), and CLM(ED) (e.g., Fisher et al., (2015), which uses the Ecosystem Demography scheme (Longo et al., 2019; Shiklomanov et al., 2021)).

The JULES model uses a similar scheme to that in CLM5, but dividing the canopy into multiple layers (the default 10 was used by Braghiere et al., (2019)). Given these contrasting results across models, we need to better understand the role of assumptions made about the 3D structure of vegetation canopies on photosynthesis. Furthermore, we note that both CLM and JULES are the land-surface schemes of CMIP-contributing Earth system models (CESM and UKESM respectively), and hence any improved understanding in these processes will also improve climate simulations.

This study tests the importance of including measured canopy structure in calculations of photosynthesis using enzyme kinetics type approaches (Collatz et al., 1992, 1991) which are commonly employed in the land surface schemes of Earth system models. The objective of this work is to test the sensitivity of modelled GPP to the common turbid medium approach to vegetation structure, and departures from it, using detailed forest canopy information. We derive a methodology to produce GPP from simulations from the high-resolution radiative transfer model, DART (Discrete Anisotropic Radiative Transfer, Gastellu-Etchegorry et al., (2015). A previous study by Demarez et al. (2000) calculated the CO_2 assimilation using DART and the Collatz et al. (1991) photosynthesis model, examining the how the distribution of LAI affected photosynthesis, however focused on a fallow field rather than a forest canopy. A more recent study by Liu et al. (2022) used TLS to explore how different canopy representations (e.g., 3D explicit and more simpler voxel-based) impact radiative fluxes.

In this work, we apply the photosynthesis scheme from a current land surface model, JULES (Clark et al., 2011), to radiative transfer calculations from DART. We are hence able to explore how different the estimates of GPP produced by a turbid medium representation of vegetation are to those of a forest canopy when different levels of canopy structure are included. Here, the resolution of the input DART scene is used as means of varying canopy structure, rather than applying a clumping factor. For six models of forest canopy plots derived from terrestrial lidar scanning (TLS), we examine the impact on the vertical profiles of the absorbed radiation, and the GPP.

A description of the DART model and the methodology to determine GPP from its radiative budget outputs are given in Section 2.1 and 2.2. The TLS data collection and sites used are outlined in Section 2.3. A comparison between JULES and DART GPP is shown in Section 3.1. Results of the comparison of GPP across scenes with decreasing horizontal resolution are given in section 3.2–3.5, with the discussion and conclusions given in Section 4 and 5.

2. Methods

2.1. Description of the discrete anisotropic radiative transfer model

The Discrete Anisotropic Radiative Transfer (DART) model (Gastellu-Etchegorry et al., 2015) computes radiative exchanges in heterogeneous Earth scenes. DART scenes are divided into grids of ‘voxels’ and ‘sub-voxels’ with an evenly spaced user-defined resolution (horizontal and vertical). Each voxel can be populated with scene elements (e.g., ground, vegetation, buildings) which are either discrete 3D objects, or turbid media. Any scene elements (e.g., vegetation or buildings) in the same voxel can interact with each other. Per-voxel radiative fluxes (absorbed, scattered, and upwelling and downwelling clear-air) can be output for each voxel.

Vegetation within DART can be represented either explicitly as individual leaves or as turbid media (Gastellu-Etchegorry et al., 2015; Janoutová et al., 2019). Describing leaves as planar surfaces, or ‘triangles’, means each individual leaf has a given area and orientation. An alternative, used in this work, is to describe vegetation as turbid media, i.e., volumes filled with randomly distributed infinitely small facets. This approach prescribes a leaf angle distribution (LAD) and leaf area volume density to the vegetation. If voxels of turbid media are distributed evenly across the scene, both horizontally and vertically, this matches the assumptions of two-stream models used in climate

simulations. Consequently, deviating from this representation, by introducing variability in space provides a means of testing the sensitivity of land models to the assumption that canopy radiative transfer can be represented by a perfectly homogeneous media.

The DART model has been widely used to model and evaluate radiative transfer in vegetation. For example, it is one of the models evaluated in the long-running model intercomparison project, RAMI (Radiative Model Intercomparison) which aims to provide a benchmark for several canopy radiative transfer schemes, examining bidirectional reflectance, as well as 1D and 3D canopy schemes (Pinty et al., 2004; Widlowski et al., 2015, 2007). Other applications of DART for vegetation include simulating airborne lidar (De Boissieu et al., 2023), modelling solar induced fluorescence (Malenovský et al., 2021; Regaieg et al., 2023), and forest fire modelling (Revilla et al., 2021).

2.2. Calculating photosynthesis using the DART model

To calculate photosynthesis from DART, we adopt the approach used within JULES. JULES is a land-surface scheme which models the exchanges of heat, momentum and mass (including water and CO_2) between soil, vegetation, and the atmosphere (Best et al., 2011; Clark et al., 2011).

A multi-layer approach to vegetation radiative transfer is used within JULES, where the vegetation canopy is divided into n equal-LAI layers (default $n = 10$). To determine the absorption and interception of radiation through the canopy, JULES uses the analytical solution to the two-stream equations for radiative transfer of Dickinson (1983) and Sellers (1985). JULES extends the Sellers approach by including sunlit and shaded leaves, through the method of Dai et al. (2004). This calculates the contribution of the uncollided incident direct beam, the scattered (or collided) component of the direct beam, and the collided and uncollided components of the incident diffuse radiation. All leaves receive the scattered component of the direct beam, and both components of the diffuse radiation incident at the top of the canopy. Sunlit leaves additionally receive unscattered radiation from the direct beam.

To compare the effect of canopy structure on the modelled photosynthesis, we apply the photosynthesis calculations from JULES to the outputs of the DART model. As the required components cannot be extracted from a single DART simulation, we develop a methodology that provides each of the terms needed for the Dai et al. (2004) solution. For each simulation, we require the amount of radiation absorbed from direct sunlight, the amount absorbed from the scattered component of the direct beam, and the amount of radiation absorbed from diffuse illumination within each DART voxel in the scene (by either leaves or soil). Hence, we complete three DART model runs for every scene:

1) A black leaf/ground, direct beam-only simulation.
2) A real leaf/ground, direct beam-only simulation.
3) A real leaf/ground, diffuse illumination-only simulation.

Here 'black' denotes a scene where an element absorbs all radiation that is incident upon them, and 'real' include scattering within the canopy. Much of this methodology follows that in Clark et al., (2011). First, for each DART voxel, we calculate L_{Sunlit}, the leaf area which is directly illuminated by the sun, using Dai et al. (2004)'s Eq. (3), from $A_{Black,Dir}$, the fraction of absorbed (A) incident light in the voxel in simulation (1):

$$L_{Sunlit} = A_{Black,Dir}/k_b \tag{1}$$

Where $k_b = G(\mu)/\mu$, G is the Ross function and $\mu = \cos(\theta_0)$, where θ_0 is the solar zenith angle. Simulations were run with a spherical LAD, ($G(\mu) = 0.5$) and a horizontal LAD ($G(\mu) = \mu$), so that we can make a direct comparison with JULES, which implements only these two LADs. We acknowledge that in real forest canopies a that these two LADs may not provide the most appropriate description (e.g. Baldocchi et al. 2002), and also that other land surface models (e.g., CLM) have more flexible descriptions of LAD.

The total LAI in each DART voxel (L_{Vox}) and the LAI that is sunlit, L_{Sunlit}, are used to calculate the sunlit fraction, f_{Sunlit}. The absorbed radiation in the real leaf/ground, direct beam-only simulation arises from both the scattered and unscattered components, hence implicitly we have:

$$A_{Real,Dir} = A_{Real,Dir,S} + A_{Real,Dir,U}. \tag{2}$$

Where $A_{Real,Dir}$ is the output DART absorption from simulation (2).

We then determine the amount of scattered radiation from the direct beam (by either leaves or soil) that has subsequently been absorbed by vegetation ($A_{Real,Dir,S}$), using both the 'black direct' and 'real direct' simulations. The $A_{Real,Dir,S}$ is equal to the absorption from the 'real direct' simulation (2) ($A_{Real,Dir}$), minus the amount of radiation that would be absorbed from the initial interception of the direct beam by the leaves ($A_{Real,Dir,U}$). This is calculated here from the absorbed radiation per voxel in the 'black direct' simulation (1), $A_{Black,Dir}$, and the leaf co-albedo, 1-ω:

$$A_{Real,Dir,S} = A_{Real,Dir} - (1-\omega)A_{Black,Dir}. \tag{3}$$

Shaded leaves intercept and absorb only diffuse radiation, both incident from the sky and scattering of the diffuse incident radiation by leaves (the sum of which is $A_{Real,Dif}$), as well as diffuse radiation due to scattering of the direct beam by leaves ($A_{Real,Dir,S}$). The absorption of these radiation streams per unit leaf area is a sum of these components weighted by the fraction of incident radiation at the top of the canopy that is diffuse, f_d:

$$A_{Shade} = \left((1-f_d)A_{Real,\ Dir,S} + f_d A_{Real,Dif}\right)/L_{Vox}. \tag{4}$$

Sunlit leaves, however, absorb both diffuse and direct radiation. Therefore, the absorption of radiation by sunlit leaves additionally includes the amount of radiation from the direct beam that is absorbed,

$$A_{Sunlit} = A_{Shade} + \left((1-f_d)A_{Real,Dir,\ U}\right)/L_{Sunlit}, \tag{5}$$

Which then simplifies to:

$$A_{Sunlit} = A_{Shade} + (1-f_d)(1-\omega)k_b. \tag{6}$$

To scale this to voxel-level absorption, A_{Sunlit} and A_{Shade} are simply weighted by L_{Sunlit} and L_{Shade} and added together.

We then use the implementation of the enzyme kinetics model for photosynthesis proposed by Collatz, within the JULES model, as described in Clark et al. (2011) to calculate GPP for each voxel using A_{Sunlit} and A_{Shade} separately. The total GPP is then given by:

$$GPP_{Total} = GPP_{Sunlit} \times f_{Sunlit} + GPP_{Shade} \times \left(1 - f_{Sunlit}\right). \tag{7}$$

Where the shaded and sunlit components of GPP (GPP_{Shade}, GPP_{Sunlit}) are calculated separately. For the purpose of coupling JULES routines into DART, we use a Python version of the JULES canopy available from the UK Met Office code repository service (https://code.metoffice.gov.uk/trac/utils/browser/leaf_simulator, last accessed 25/03/24).

The JULES canopy simulator implements all leaf level aspects of photosynthesis that are in the full JULES model, and which are needed to calculate the sunlit and shaded GPP components in Eq. (7). Full energy and mass balance are not represented, however, and hence the simulator does not include prognostic soil moisture or leaf temperature. In this manuscript we set the soil moisture such that there is no impact on photosynthesis, and leaf temperature is input to the model as described in the individual experiments. Photosynthesis calculations closely follow the approach described by Collatz et al. (1991) in which carbon assimilation is the minimum of possible assimilation rates from light, Rubisco, and transport limitation. Full details are given by Clark et al. (2011).

For the photosynthesis calculations we vary the leaf temperature

(T_{Leaf}), incoming photosynthetically active radiation (IPAR) and θ_0 to identify how the relationship between structure and GPP may change with environmental conditions.

These environmental parameters along with f_d are varied throughout the study. Within JULES, the value of V_{cmax} – the maximum rate of carboxylation, a key parameter in the photosynthesis calculations – is determined by the values of T_{Leaf} and the value of V_{cmax} at 25 °C (V_{cmax25}). The V_{cmax25} is a function of leaf nitrogen or, in simulations where there is no active nitrogen cycle (as in this work), it is prescribed on a PFT basis. As the T_{Leaf} is prescribed the same for both sunlit and shaded leaves, V_{cmax} is also the same for both.

For the photosynthesis calculations, a range of realistic temperatures are selected, so $T_{Leaf} = 10, 15, 20, 25, 30$ °C. This corresponds to values of $V_{cmax} = 0$, 2.0×10^{-6}, 1.17×10^{-5}, 5.4×10^{-5}, 2.31×10^{-4}, 9.19×10^{-4} mol CO_2 m^{-2} s^{-1}. Values of IPAR are selected between 100 W m^{-2} and 400 W m^{-2}.

2.3. Real forest canopies in DART

2.3.1. TLS data

This study assesses the implications of canopy structure for GPP calculation across six forest plots where TLS data has been previously collected (Table 1). These are: Nova Xavantina (Brazil), Eifel (Germany), Harvard (USA), Lopé (Gabon), Maliau (Malaysia), Wytham Woods (UK) (Fig. 1). Sampling across these six sites means that we capture multiple habitat types, including savannah, tropical forest, mixed temperate forest (conifer and deciduous), and spruce. The total LAI range across the scenes is 2.22 m^2 m^{-2} (Eifel) - 6.48 m^2 m^{-2} (Maliau), and the maximum height ranges from 12 m - 98 m.

For all sites, TLS data were collected using the sampling protocol of Wilkes et al. (2017). All scanning was conducted with a RIEGL VZ400 (RIEGL, Horn, Austria) where scan rate was 300 KHz and angular step was 0.04°. Scans were captured on a regular grid (Table 1) where at each scan position an upright and a tilt scan were acquired. Scans were co-registered using a set of targets as tie-points (Wilkes et al., 2017) using the RiSCAN Pro software package. The finest spatial resolution used for most sites is the grid size that the TLS data were captured on. This is not the case for Eifel, where the plot has been scaled to 25 m × 25 m so all DART 1 m × 1 m are filled with turbid media, and for Wytham Woods where supplementary data means that the spatial resolution of the LAI can be determined at 1 m × 1 m.

2.4. Calculating leaf area index from TLS data

For all sites, a spatially explicit estimate of LAI was derived and voxelised. Two different methods were used to calculate LAI. For all plots, LAI was computed using the method of Jupp and Lovell (2007) where vertically resolved Plant Area Volume Density is determined from TLS derived gap probability (Calders et al., 2014).

Due to the availability of additional data, a second method to determine LAI was applied only at Wytham Woods. This method involved aggregating and voxelising leaf facets from an existing radiative transfer model (Calders et al., 2018). The LAI for the this existing model was estimated from hemispherical photography (Calders et al., 2018).

2.5. DART settings

All radiative transfer simulations in this study use DART in 'forward' flux-tracking mode, based on the discrete-ordinate method (Gastellu-Etchegorry et al., 2015). Broadband simulations are completed within the PAR region of 0.4 – 0.7 μm. DART simulations track radiation along 12 directions within the 4π space, with three iterations completed. No atmosphere is prescribed within DART for this study.

Here, all vegetation elements are set as turbid media (Section 2.1), with the voxel LAI determined from TLS (Section 2.3.1). DART voxels are set to have vertical and horizontal resolutions of 1 m in all simulations. The JULES model does not consider stem or branch structures within forest canopies, and so, despite the ability of the DART model to consider these, in this work we neglect them, to maintain consistency with the land surface modelling approach. Scenes are set within DART to be repetitive. The six plots have no underlying topographic variation, which is consistent with the assumptions used in the canopy radiative transfer calculations of most common land surface modelling approaches, however at the plot scale used here (> 100 m) the impact of the true topography on the vegetation and radiative fluxes is likely to be small.

We assume that all vegetation within each plot has the same optical properties, mirroring the assumptions inside land models like JULES (which typically prescribe uniform optical properties across PFT) and allowing us to isolate the sensitivity of GPP predictions to canopy structure alone. For "black" simulations, the albedo of all surfaces (leaves and ground) are set to 0, to absorb all incident radiation. For 'real' simulations the leaf properties are set for a typical JULES PFT, assuming the ground albedo = 0.1, and leaf reflectance = 0.1, and leaf single scattering albedo = 0.15. All simulations are set with these same optical properties so that any variability arises from the structure only. Although this assumption is consistent with those made in land surface models, it neglects real-world spatial variability in optical properties within tree canopies. In effect, this assumes that the mean leaf optical properties will lead to a representative value of fAPAR for the whole canopy, which is likely a suitable first-order approximation but could be an avenue for future research.

Within this work we complete a sensitivity test to environmental conditions. The only parameter that is specified within DART for this is the θ_0, and we sample five from directly overhead sun to a low sun angle of 60°, sampling every 15°.

3. Results

3.1. Reproducibility of JULES canopy simulator output

We test out GPP calculations using a canopy with constant vertical LAI and no horizontal LAI variation, against identical simulations from the JULES canopy simulator using the Sellers two-stream model. We compare profiles of both the fraction of absorbed PAR (fAPAR) and GPP for the sunlit and shaded parts of the canopy. Both models are run using multiple f_d and θ_0 (Fig. 2). Within these simulations we use the LAI of the Wytham simulations (L = 3.65 m^2 m^{-2}), where both DART and JULES are run with 10 equal-LAI vertical layers, each with an L = 0.365.

Table 1
Details of forest plots used in this study, including location (latitude/longitude), total scene leaf area index (LAI), collected TLS resolution and plot size, maximum height collected (H_{Max}), and dominant tree type within the plot.

Plot	Lat	Lon	Plot size (*d, m*)	TLS resolution (m)	LAI (m^2 m^{-2})	H_{Max} (m)	Forest type
Wytham Woods	51.773	-1.322	100	20	3.65	30	Temperate broadleaf
Maliau	4.745	116.970	100	10	6.48	98	Tropical rain forest
Nova Xavantina	-14.713	-52.354	100	10	3.03	12	*Cerrado tipico*
Harvard	42.5120	-72.2189	60	10	5.10	32	Transition Hardwood
Lope	-0.174615	11.573313	100	10	3.34	44	Tropical rain forest
Eifel	50.615	6.433	66.4	16.6	2.23	35	Beech plantation

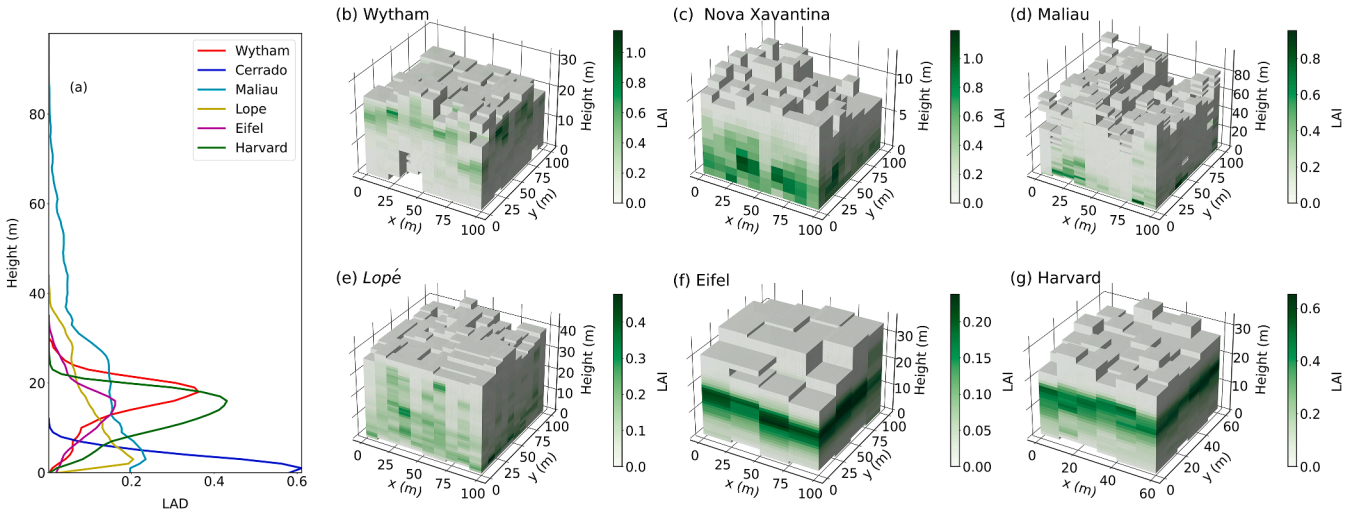

Fig. 1. (a) Vertical profiles with height, and 3D structure of LAD within six forest canopy plots, (b) Wytham Woods, (c) Nova Xavantina, (d) Maliau, (e) Lopé, (f) Harvard, and (g) Eifel, derived from terrestrial laser scanning (TLS). All plots are shown at their scanned resolution (e.g., Nova Xavantina at 10 m × 10 m, Table 1), except Wytham Woods which is shown at 10 m × 10 m, and Eifel which is shown at a scaled resolution of 25 m × 25 m.

Across all f_d and θ_0 sampled, the JULES and DART simulations show almost identical profile shapes for both GPP and fAPAR (Fig. 2, Fig. S2). The results are consistent across all values of θ_0 sampled, with only two values shown in Fig. 2 for simplicity (θ_0, = 15°, 45°, 60°, shown in Fig. S2). For both entirely diffuse and direct simulations (f_d = 1.0, 0.0), we see slight disagreement at the base and top of the canopy. This contrasts with simulations where $f_d = 0.5$, where there is agreement at the top and base of the canopy but disagreement within, where DART has lower GPP and fAPAR than in JULES.

When $f_d = 0.0$, DART is lower than JULES for both fAPAR and GPP in the lower canopy, the relationship flipping when cumulative LAI < 1.0. The opposite is the case when $f_d = 1.0$, with DART lower than JULES in the upper canopy for both fAPAR and GPP (LAI to ~ 2.5 m^2 m^{-2}). Because the differences apparent in fAPAR are always < 2.5 %, we assume they arise due to differences in the radiative transfer solutions between DART and the Sellers two-stream model. Differences in GPP are driven by these differences in absorbed radiation because the onward calculations are identical (using the same Python code).

3.2. Spatial resampling of DART scenes

We modify the spatial resolution to determine the impact of the horizontal structure on the total canopy GPP. The resolution is coarsened from the original resolution of the TLS sampling or DART scene (v) to the plot size. In the latter case, this would produce a scene that is similar to the setup used within JULES, but with a non-homogenous vertical distribution of the LAI. Here, we average the LAI horizontally such that a single LAI value is used for the entire horizontal extent of the scene, e.g., for Wytham, the scene is coarsened at 2 m, 5 m, 10 m, 20 m, 50 m, and 100 m resolution. For Harvard, which has a plot diameter, d = 60 m, v = 10 m, the only other resolutions we can resample the LAI at are 20 m and 30 m.

As the canopy structure is coarsened, the scenes looks less realistic. This is most notable for Wytham (Fig. S1), which is collected at the finest resolution, where the gaps in the canopy towards the ground, and the emergent vegetation at the canopy top, are removed as the resolution is coarsened (Fig. S1).

Although more visible for Wytham Woods (as the model is down sampled from an existing model), we see fewer sub-canopy gaps where radiation could penetrate to ground level in all scenes as the resolution is coarsened (Fig. 3). In all scenes the total LAI remains the same through each level of degradation. Key features of the forest structure, such as the two areas of dense vegetation in the Maliau scene are lost when we capture the LAI distribution at a higher resolution (Fig. 3). This contrasts with the Cerrado scene, where forest succession has caused the vegetation to be taller on one side of the plot to the other, and so the reduction in height and LAI across the canopy can still be seen at v = 50 m. Forest plots that are more horizontally homogenous (e.g., Eifel and Harvard, Fig. 4), have less obvious changes in LAI as the spatial resolution is coarsened (Fig. 3).

3.3. The impact of voxel resolution on vertical properties - Wytham Woods

We examine the vertical profiles of fAPAR, and GPP for both sunlit and shaded leaves for Wytham Woods. We examine the profiles for θ_0 = 0°, and for IPAR = 100, 300, 500 W m^{-2}.

Across the resolutions sampled for Wytham, we see three archetypes of behaviour from the fAPAR and GPP profiles (Fig. 5). These are a result of averaging across multiple columns in the scene, each of which describes a different exponential decay in absorbed radiation through the canopy. For the 100 m × 100 m scene, each fAPAR profile start at the same height, with the same LAI profile, and so look similar to those from JULES (Fig. 2). As the scenes become more realistic, there are larger differences in the LAI profiles, but also the height in the scene the profile starts from, changing the average.

The first type of behaviour is seen for v = 1 m, the highest spatial resolution, where the fAPAR or GPP at any cumulative LAI is always the smallest (cf. any other resolution). For the v = 1 m and 10 m, we see the fAPAR at the top of the canopy fall to zero, as a result of small but dense voxels of vegetation present above the main surface of the canopy. These are the areas of emergent vegetation at the top of the canopy seen in Fig. S1 and contrast with the horizontally homogenous canopies where the largest fAPAR is seen at the top of the canopy.

The second type of profile, seen when $v \geq 10$ m, shows a higher fAPAR further towards the top of the canopy, but lower than that of the horizontally homogenous canopies. The greatest fAPAR and GPP magnitudes are seen close to the canopy top, but then rapidly drop down to zero at the canopy top (as when v = 1 m). The third profile, from the horizontally homogenous canopy (v = 100 m) exhibits a profile like that seen in JULES (Section 3.1).

In all simulations the fAPAR and GPP in the shaded part of the canopy is always lower than the sunlit part. As the IPAR increases, the maximum GPP increases in all canopies. The scene where v = 1 m shows a curved sunlit GPP profile, which has a small area of near-constant GPP in the centre of the canopy (by LAI) when GPP increases. However, when

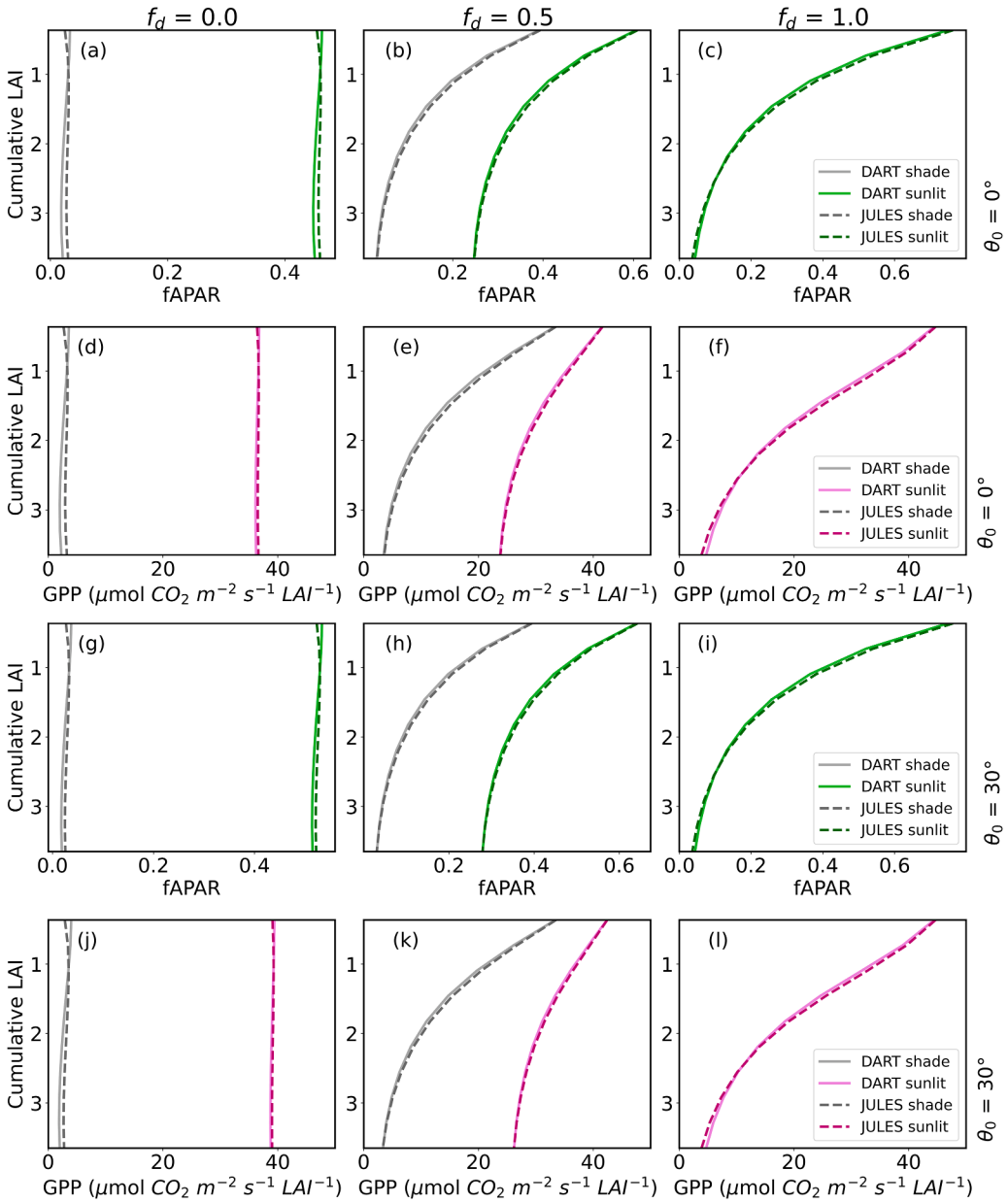

Fig. 2. Comparison of the sunlit (solid) and shaded (dashed) profiles of fAPAR and GPP for a slab canopy with homogenously distributed L = 3.65 m^2 m^{-2} across 10 layers in DART (black) and the JULES canopy simulator (blue). Both simulations are conducted for three fractions of diffuse radiation, f_d = 0.0, 0.5, 1.0, and for two solar zenith angles, θ_0 = 0°, 30°. In all of these experiments, T_{Leaf} = 25 °C, and IPAR = 300 W m^{-2}

the IPAR increases in both the ν = 10 m, 100 m scenes, the sunlit GPP becomes almost constant with depth, with the ν = 10 m canopy ~ 43 μmol CO_2 m^{-2} s^{-1} LAI^{-1} between a cumulative LAI ~ 0.75 – 3.3 m^2 m^{-2}.

3.4. Impact of canopy resolution on total GPP

The effect of varying the horizontal resolution of the canopy is tested across all six forest plots (Fig. 1) at all resolutions (Fig. 3), for a range of IPAR, θ_0, f_d, and T_{Leaf}. The selection of environmental parameters tested are given in Section 2.4.

The vertically integrated GPP across all scenes for a given selection of environmental parameters shows spatial patterns consistent with the integrated LAI (Fig. 3); with the areas of largest GPP having the largest LAI (Fig. 6). As we coarsened the voxel resolution, the spatial variability of GPP decreases, as would be expected. This is the clearest in the Wytham Woods plot, as when the LAI is coarsened, the fraction of open space in the canopy decreases, leading to a more even GPP across the scene.

Taking scenes only with illumination at nadir, with an optimum T_{Leaf} = 25 °C, the total canopy GPP across all plots and resolution increases as the IPAR increases (Fig. 7, Fig. S3). Generally, in these cases, for any scene, the total canopy GPP is highest for the 100 m × 100 m canopy (60 m × 60 m, Harvard), and lowest for the finest resolution scene (Fig. 7). This is most evident across the range of resolutions in Wytham Woods and Maliau, with slight differences in Nova Xavantina and Lopé. Larger differences between resolutions can be seen when the IPAR is highest. This may be due to the spatial heterogeneity of the forest plots, as the scenes with the highest variability in the total canopy GPP are those that have higher horizontal variability in the LAI (Fig. 4).

Given results from other studies (e.g., Braghiere et al. (2019); Li et al. (2023)), which show that GPP increases when canopy structure is introduced, we examine the above across IPAR and T_{Leaf} for all scenes with a range of f_d (Fig. S4 – Fig. S8). We find that in almost all cases, that more detail in structure (i.e., finer resolution simulations) decreases GPP. For Wytham Woods, when f_d = 0.5, this can be up to 15.5 %

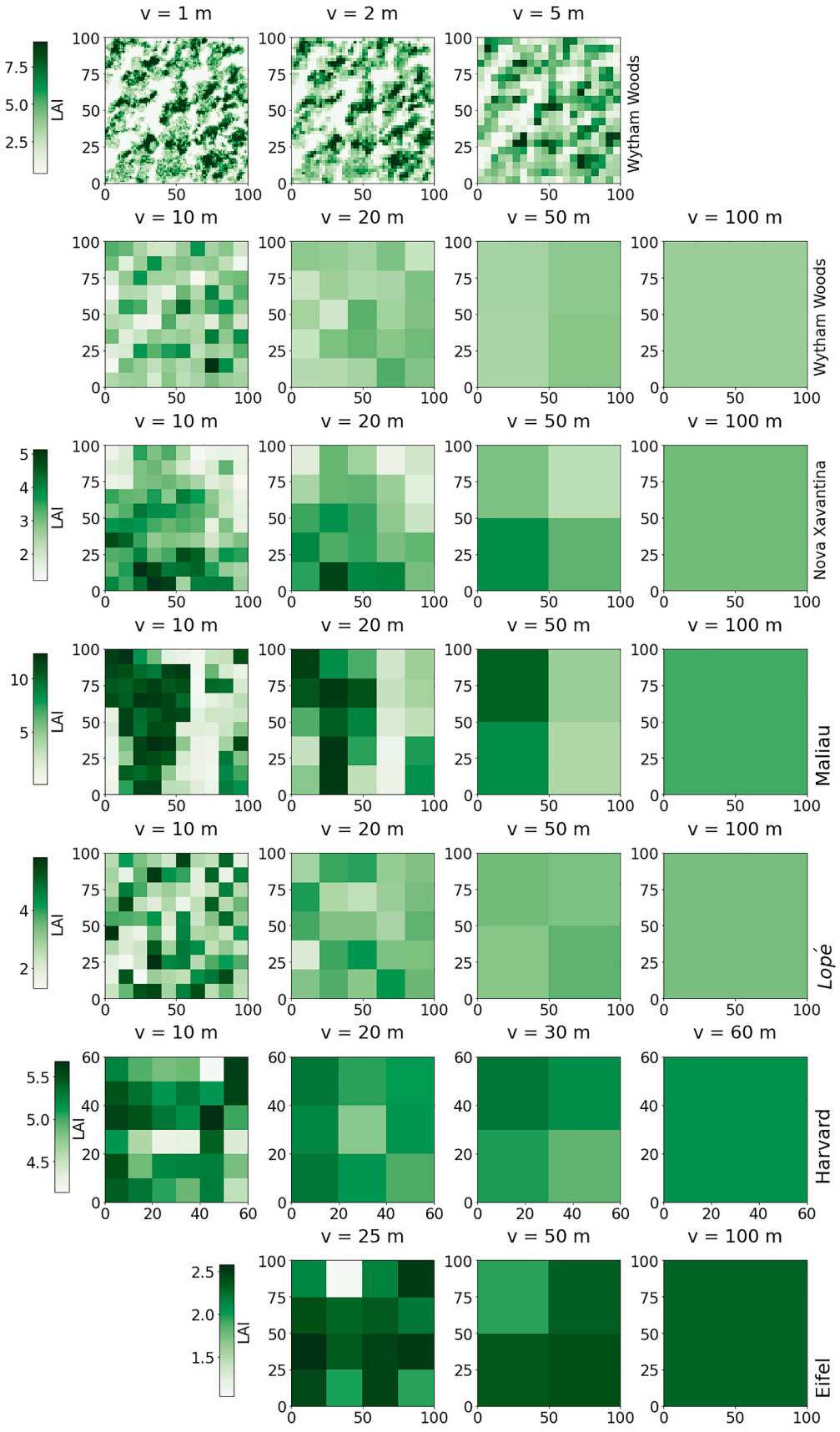

Fig. 3. Vertically integrated LAI for each of the six forest plots (Row, Fig. 2, Table 1), for each resolution in this study (column).

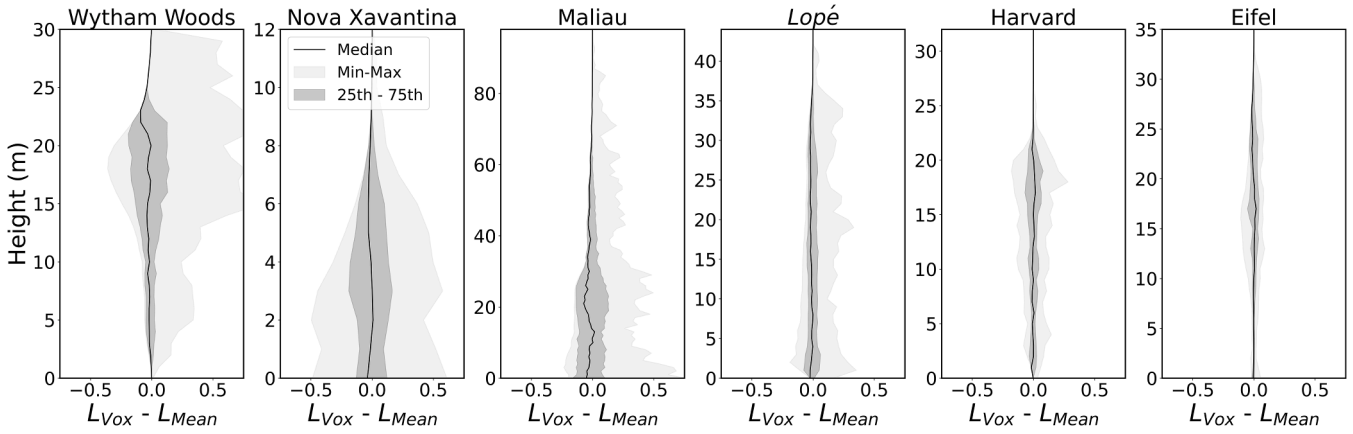

Fig. 4. Difference between the voxel LAI (L_{Vox}) and the mean layer LAI (L_{Mean}) for six forest plots (Fig. 1), with the median (solid line), IQR, and minimum and maximum difference shown. All plots are shown at the captured TLS resolution (Table 1), except Wytham Woods which is shown at 10 m × 10 m.

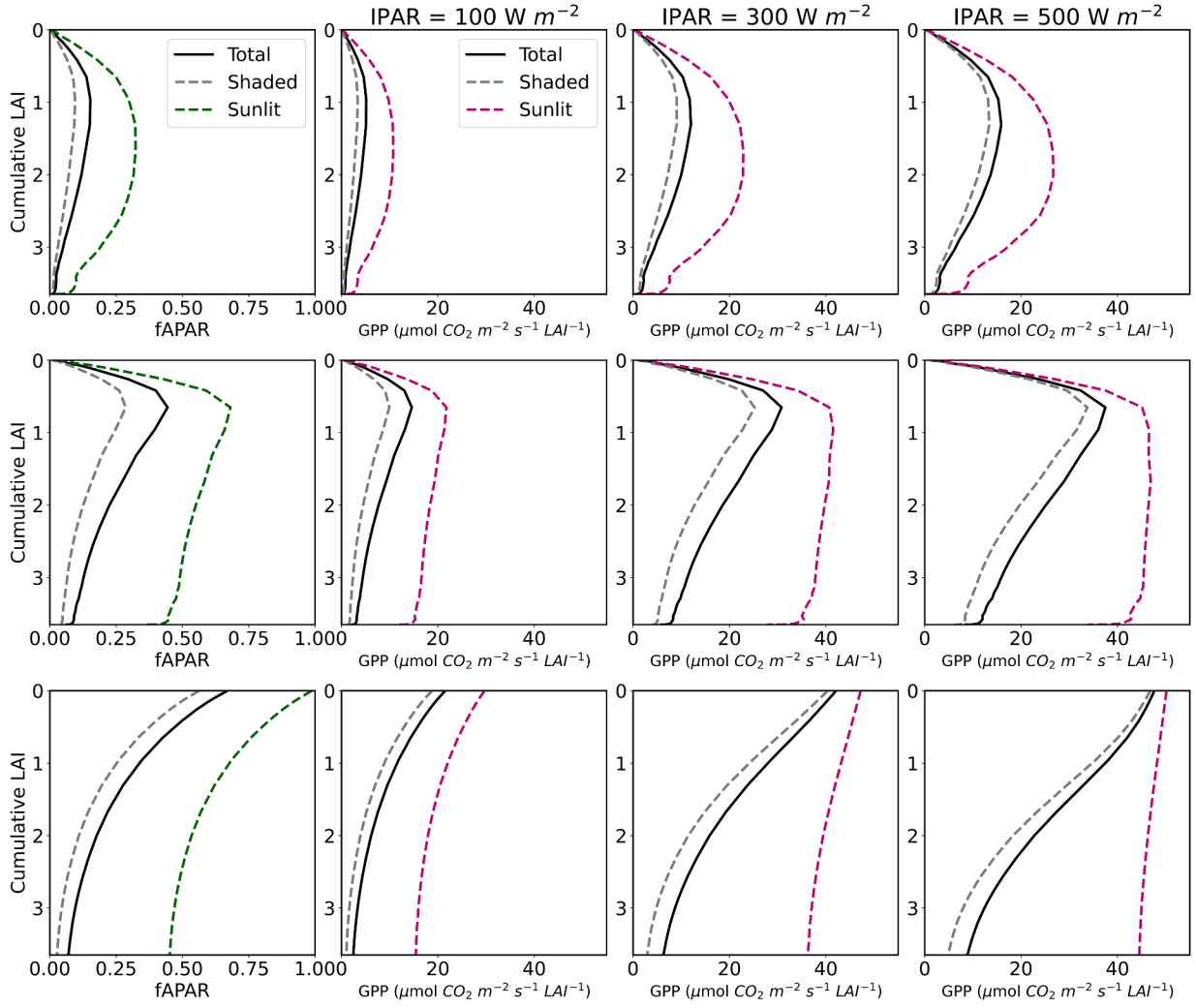

Fig. 5. Vertical profiles of sunlit (green, dashed), shaded (grey, dashed) and total (black, solid) canopy absorption (fAPAR, column 1) and GPP (pink, columns 2–4) for Wytham Woods at three resolutions (rows: 1 m, 10 m, 100 m) for overhead sun ($\theta_0 = 0$), with GPP calculated using $f_d = 0.5$ and $T_{Leaf} = 25$ °C, across three values of IPAR.

difference, with the largest differences seen at high temperatures. A few exceptions occur when GPP does increase, however the magnitude of the change is much less (< 1 %). There are 24 exceptions when $f_d = 0.5$ and $\theta_0 = 0°$, across the range of IPAR and T_{Leaf} tested, but generally at lower values of T_{Leaf}, which occur at coarser resolutions (v = 20, 50 m). Examining other values of f_d, we find similar results, with decreases in GPP up to 25 % when $f_d = 0.0$ for Wytham Woods. Similarly, we see increases in GPP for this same case of up to 2.3 %. However, we note that a case where all incoming radiation is completely from the direct beam is uncommon.

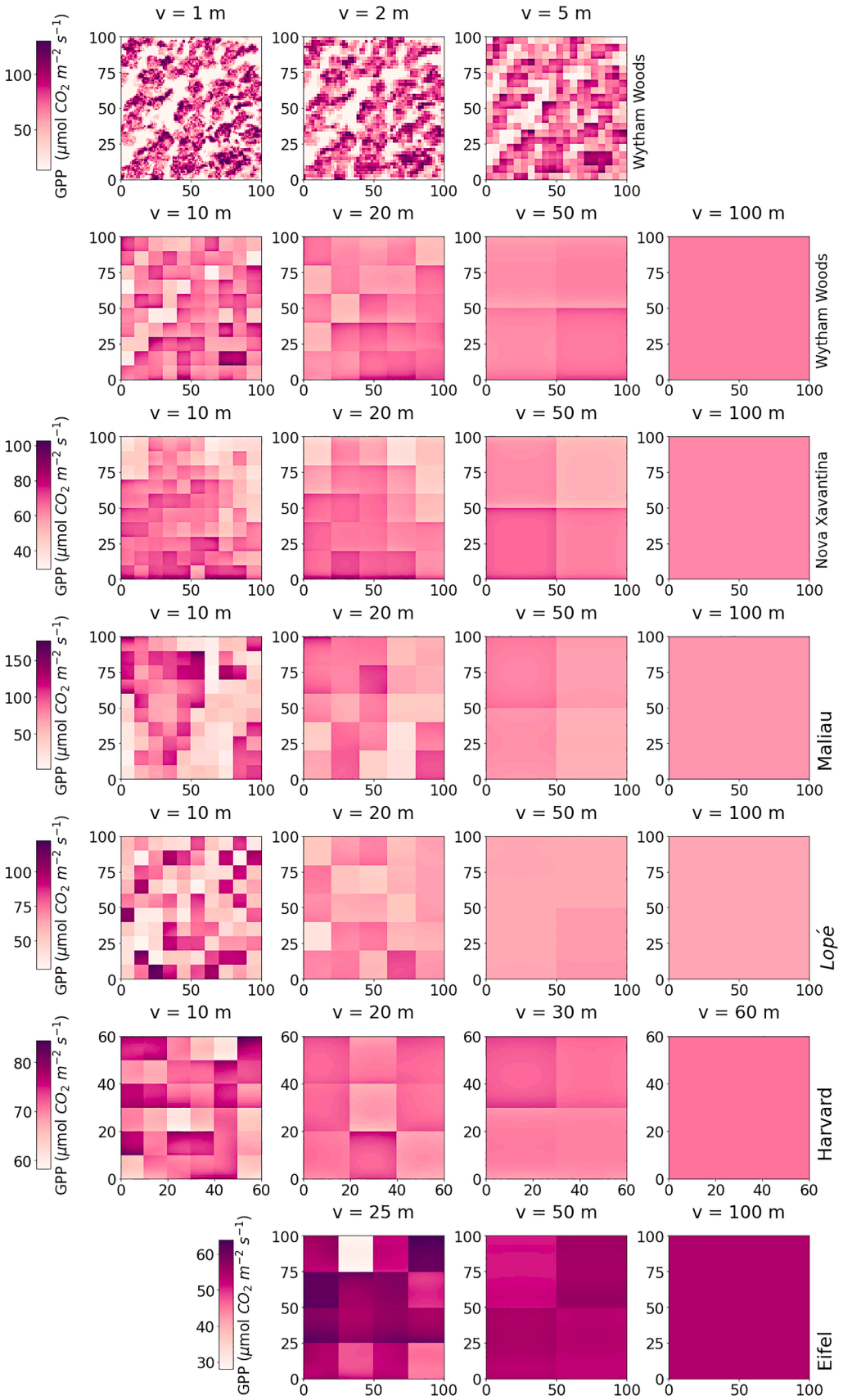

Fig. 6. Vertically integrated GPP for six forest plots (Fig. 1, Table 1) for IPAR = 300 W m^{-2}, $\theta_0 = 0$, and $T_{Leaf} = 25°$. All scenes are coarsened at different resolutions due to the plot size and the available TLS resolution (Table 1).

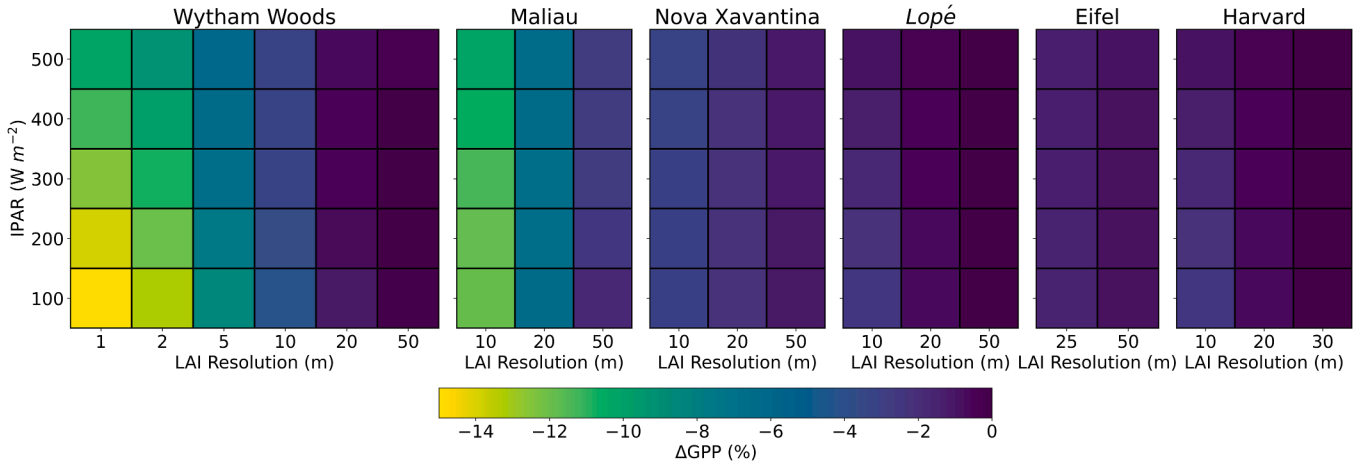

Fig. 7. The difference in total canopy GPP between each coarsened spatial resolution (Fig. 1, Fig. 3) and the slab canopy (ΔGPP), for each of the six forest plots for a single solar zenith angle, $\theta_0 = 0°$ and leaf temperature, $T_{Leaf} = 25$ °C, for a range of IPAR.

The relationships mentioned above also hold across sun angle changes (Fig. 8); however, this is less pronounced, with lower θ_0 producing a lower difference in the total GPP across scenes. Although we test six values of θ_0 only three are shown for each site, for clarity as the same relationships are found across all θ_0. In scenes where there is a larger range of GPP across spatial resolution in Figs. 6 and 7 (e.g., Wytham Woods and Maliau), the range across θ_0 remains largest across low sun angles. This decrease in GPP with a lower sun likely occurs as there is less penetration of radiation through canopy gaps that are opened up due to the use of finer canopy structure.

3.5. Sensitivity of GPP relations to canopy parameter choice

To understand whether the results shown in this paper are independent of the parameter choices made, extra simulations have been completed focusing on three specific parameters sets that influence the interaction of leaves with radiation: LAI, optical properties, and LAD. The first of these use all six sites, and isolate the structure-only effects,

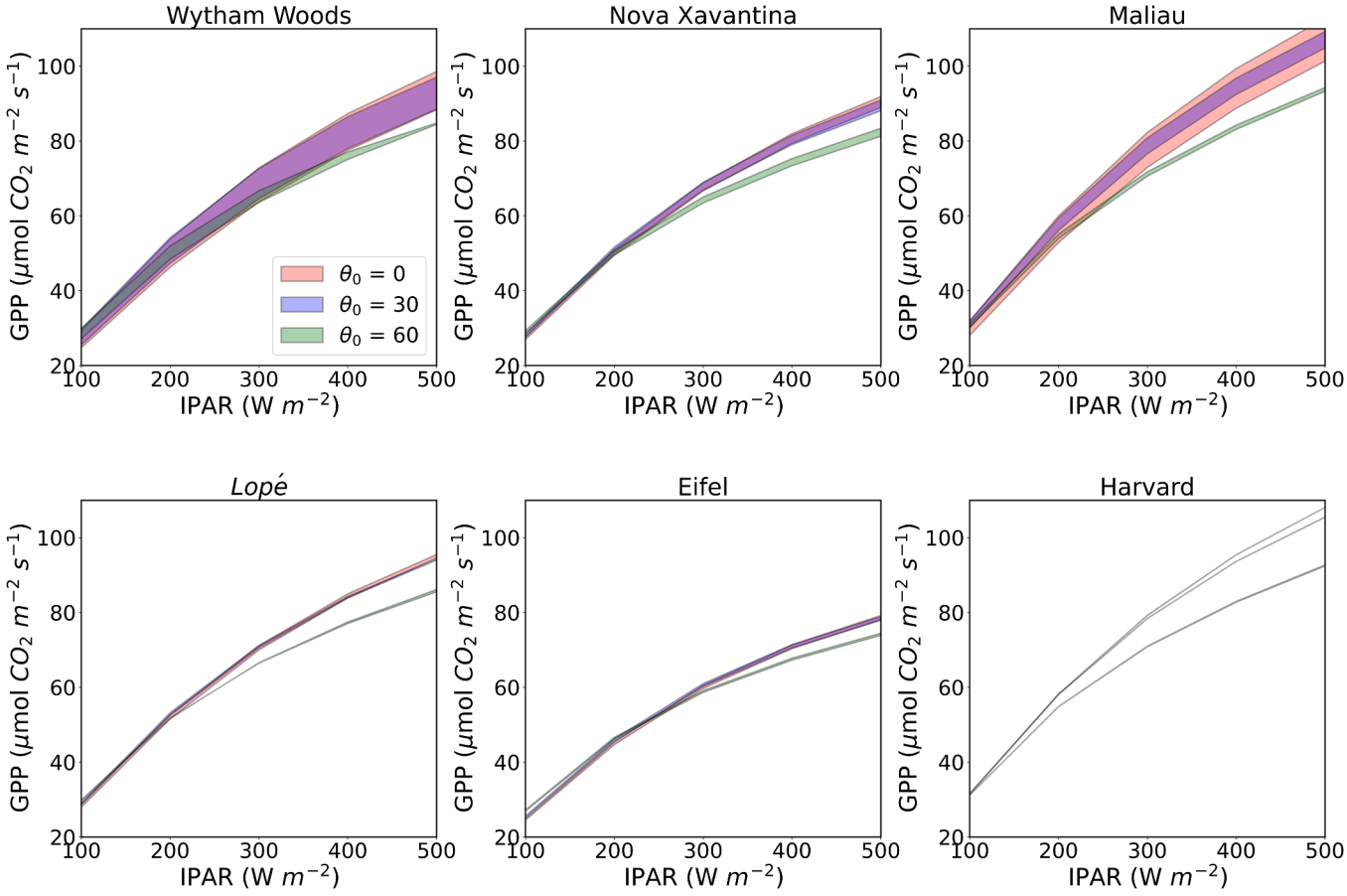

Fig. 8. The range of total canopy GPP across LAI resolution for (a) Wytham Woods, (b) Nova Xavantina, (c) Maliau, (d) Lope, (e) Eifel, and (d) Harvard. Each resolution is simulated with a range of IPAR, and three solar zenith angles, $\theta_0 = 0°$, 30°, 60°, with leaf temperature, $T_{Leaf} = 25$ °C.

by scaling each canopy LAI so that all scenes have the same LAI. The latter two experiments use only the Wytham Woods site at three resolutions ($v = 1$ m, 10 m, and 100 m).

3.5.1. Magnitude of the scene LAI

The work in section 3.4 examines the variability of total canopy GPP across multiple scenes and environmental conditions, however all scenes have differing total canopy LAI. Here, we expand on this and isolate the structure-only effects, by scaling the total LAI of each scene such that $L = 3.0$ m^2 m^{-2}, whilst retaining the spatial distribution of LAI. The DART simulations are then completed for all resolutions of the forest canopies. To further remove the influence of LAI on the canopy GPP, the Wytham Woods LAI is scaled to $L = 1.0$, and $L = 10.0$. at three resolutions ($v = 1$ m, 10 m, 100 m).

Firstly, in the horizontally homogenous simulations (Fig. 9, bars labelled 100 and 60), the vertical variability of LAI has no influence on the total canopy GPP. Despite differences in the vertical profiles of LAI (Fig. 1), the total GPP across all scenes are roughly equal.

The largest differences in GPP across the simulations where $v = 10$ m – 100 m are found in the Maliau simulations (Fig. 9). Here, for constant IPAR and T_{Leaf}, the differences in GPP between the coarsest and finest resolutions are ~ 7 µmol CO_2 m^{-2} s^{-1} This is also seen in Fig. 7. This is likely due to the sharp gradient in the LAI across the scene (Fig. 3).

Although Wytham shows a similar change in GPP across the spatial resolutions (1 m – 100 m) as Maliau, the change from 10 m – 100 m is only small (> 3 µmol CO_2 m^{-2} s^{-1}). This is similar to both Nova Xavantina and Lopé, although the Nova Xavantina GPP always decreases with spatial resolution. In contrast, the Wytham and Lopé GPP are almost identical between $v = 50$ m and 100 m. These three scenes show varying amounts of horizontal variation of LAI, with Nova Xavantina showing an LAI spread ~ 1 for half of the canopy, Wytham showing an LAI spread of ~ 0.5 m^2 m^{-2}. Some scenes show almost no variation of GPP with canopy structure (Eifel, Harvard, Fig. 9). This is consistent with the results in Section 3.4.

In the simulations for Wytham, there is a large change in the GPP between the case where $v = 20$ m, and $v = 1$ m (Fig. 9). This could point to a difference in behaviours captured by the simulations as the spatial resolutions becomes finer, for example from crown scale at the coarser resolutions, to branch scale when $v = 1$ m of 2 m.

The additional simulations for Wytham Woods (Fig. 10) suggest that the pattern of decrease in GPP between the homogenous canopy and the finest spatial structure is consistent between the different LAI magnitudes. The GPP for all resolutions is significantly larger in the scenes with higher LAI, as expected, with almost double the GPP between $L = 1.0$ and $L = 10.0$. The difference between the finest spatial structure and the homogenous canopy is much larger in the simulations with higher LAI (Fig. 10b, c), with a similar magnitude difference between $v = 1$ m and $v = 10$ m in the simulations with $L = 3.0$ and $L = 10.0$ (~ 7 µmol CO_2 m^{-2} s^{-1}).

3.5.2. Leaf and soil optical properties

To determine whether our findings in Section 3.4 are sensitive to optical properties of leaves and soil, we carried out two experiments using the data from Wytham Woods at three spatial resolutions. The first of these used higher values of leaf albedo and transmittance (both 0.2). The second used an enhanced soil albedo of 0.3.

The simulations where the soil albedo is increased have increased total GPP compared to simulations with the original optical properties, denoted "JULES PFT" (Fig. 11). This is expected as the soil reflects more radiation back towards the leaves which then absorb more, leading to more GPP. In contrast, the simulations where the leaf albedo and transmittance are increased have a lower GPP than the simulations using the JULES PFT values, simply because the leaves are absorbing less radiation.

Both simulations follow the results in section 3.4, that the canopy total GPP is lowest when a finer resolution, and hence greater detail on canopy structure, is used. As the simulated θ_0 increases (off-nadir) the total GPP generally increases, as in Fig. 8. This is most consistent in the $v = 1$ m simulations. In the other resolutions, the GPP starts to decrease at the higher θ_0 (45° or 60°). The simulations where soil albedo is modified become closer to the original simulations when the sun is lower in the sky as less radiation penetrates to ground level and hence less radiation can be reflected back into the canopy.

3.5.3. Leaf angle distribution

To examine whether our findings in Section 3.4 would change under different leaf angles, we complete a further experiment using Wytham Woods at three spatial resolutions. In these simulations we implement a

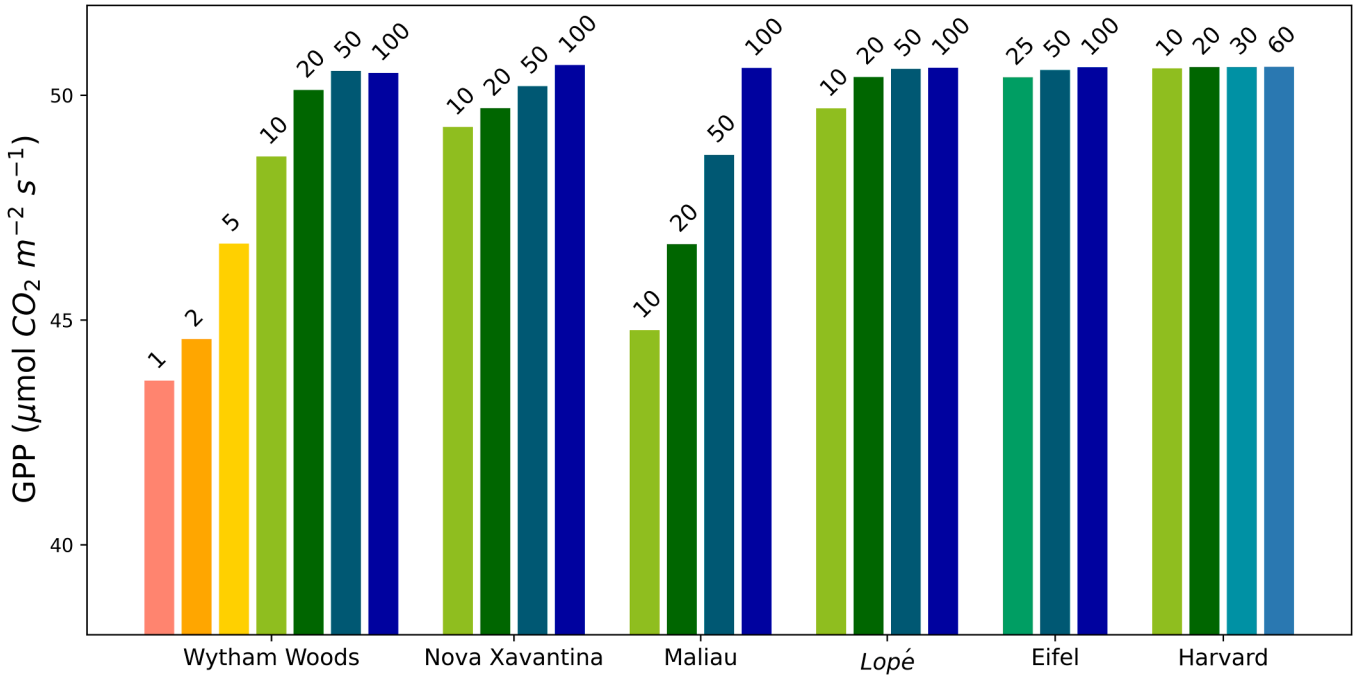

Fig. 9. The total canopy GPP for each forest canopy used here, but with the scene LAI, L = 3.0, for all spatial resolutions used in the study (Fig. 3). All $\theta_0 = 0°$.

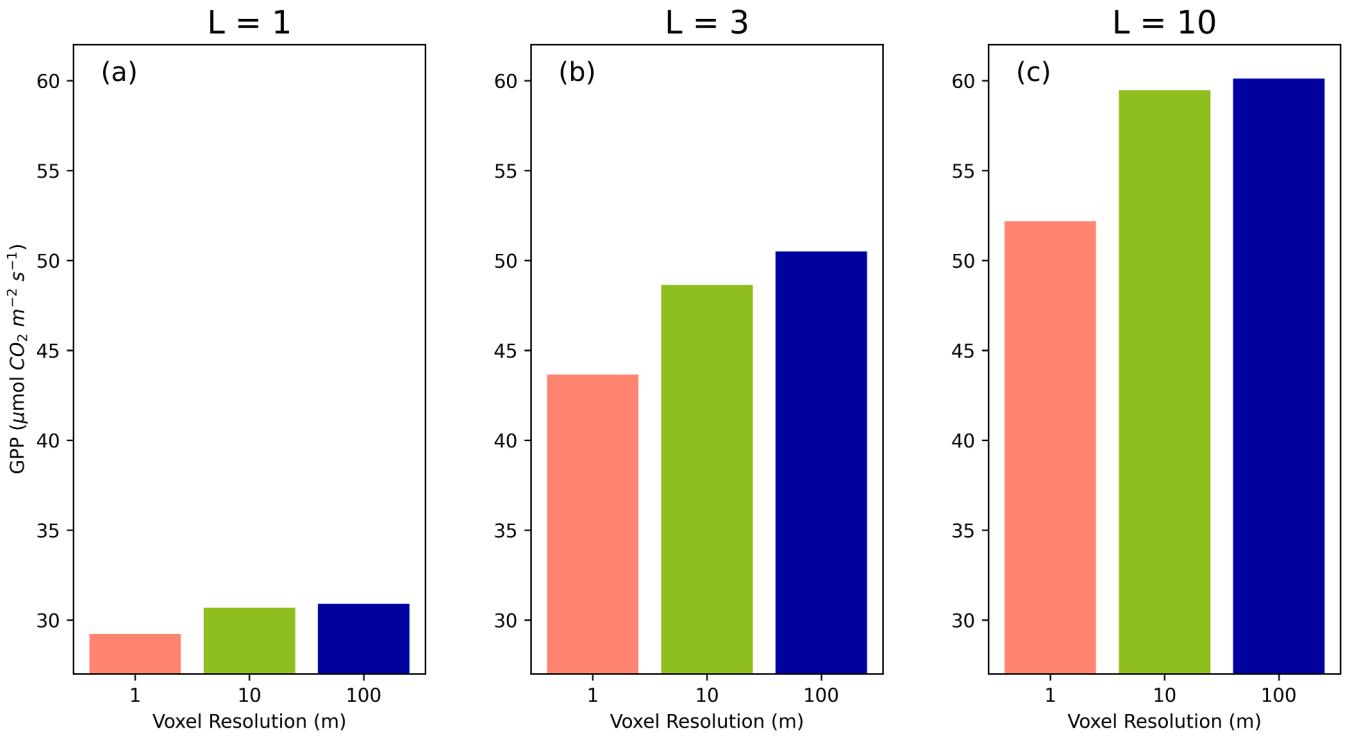

Fig. 10. The total canopy GPP for Wytham Woods at three resolutions (1 m, 10 m, 100 m, Fig. 1, Table 1), but with the scene LAI normalised to three values, (a) L = 1.0, (b) L = 3.0, (c) L = 10.0, for all spatial resolutions used in the study (Fig. 3). All $\theta_0 = 0°$.

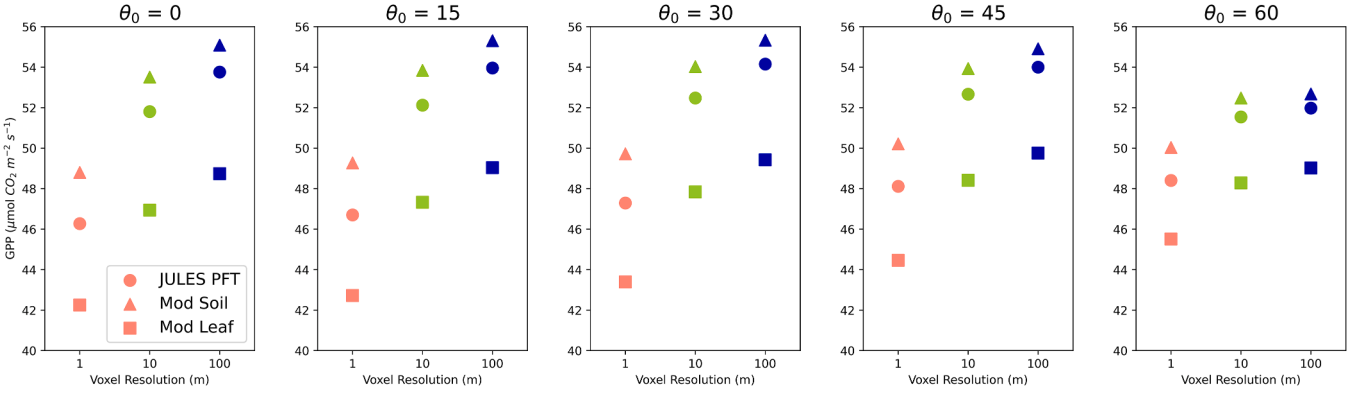

Fig. 11. The total canopy GPP for Wytham Woods at three resolutions (v = 1 m, 10 m, 100 m, Fig. 1, Table 1), but with optical properties of both soil (triangle) and leaves (square) modified, across five solar zenith angles, $\theta_0 = 0°, 15°, 30°, 45°, 60°$, with leaf temperature, $T_{Leaf} = 25$ °C and IPAR = 200 W m^{-2}.

horizontal LAD, which is the only alternative in the JULES model to the spherical LAD.

The simulations with horizontal LAD show the scene GPP is decreased at Wytham Woods when the finest spatial resolution is used (Fig. 12). As in Fig. 8, the total scene GPP decreases as θ_0 increases. However, the difference in the GPP across θ_0 is minimal (~ 2 μmol CO_2 m^{-2} s^{-1}). The homogenous scenes show little difference in canopy GPP across θ_0 until $\theta_0 = 60°$, when there is a decrease in GPP. A similar, but less marked pattern is seen when $v = 10$ m.

4. Discussion

Despite the importance of terrestrial vegetation to the carbon cycle, there are large uncertainties in the magnitude of the global primary productivity (GPP) flux. For climate models, one source of uncertainty in GPP predictions, which we argue is significant, is the simplicity with which vegetation structure is represented. Here, we introduce a methodology to calculate GPP from a radiative transfer model, DART (Gastellu-Etchegorry et al., 2015), which can represent the canopy at arbitrary levels of detail given appropriate input data. Using this methodology, we investigated the effect on modelled GPP, of incorporating varying levels of explicit canopy structure rather than commonly used clumping factors which scale the bulk LAI of the canopy. The input data on the spatial distribution of leaves was derived from terrestrial laser scanning (TLS), which was translated into the leaf density per voxel for input to DART, and then the horizontal resolution was varied from the finest we could reliably calculate with the data collected, to a representation like that seen in a typical climate model land surface scheme.

Modifying the horizontal voxel resolution changes the vertical profile of both fAPAR and GPP within the forest canopy. We find three archetype profiles. The most detailed TLS (1 m) leads to a GPP curve that starts and ends at 0 μmol CO_2 m^{-2} s^{-1} LAI^{-1}, indicating areas of emergent vegetation at the top of the canopy that are seen in the TLS data, and at the bottom openness under the tree crowns themselves. The second archetype shows values of mean GPP (and fAPAR) 0 μmol CO_2 m^{-2} s^{-1} LAI^{-1} at the canopy top, with the highest fAPAR/GPP towards the

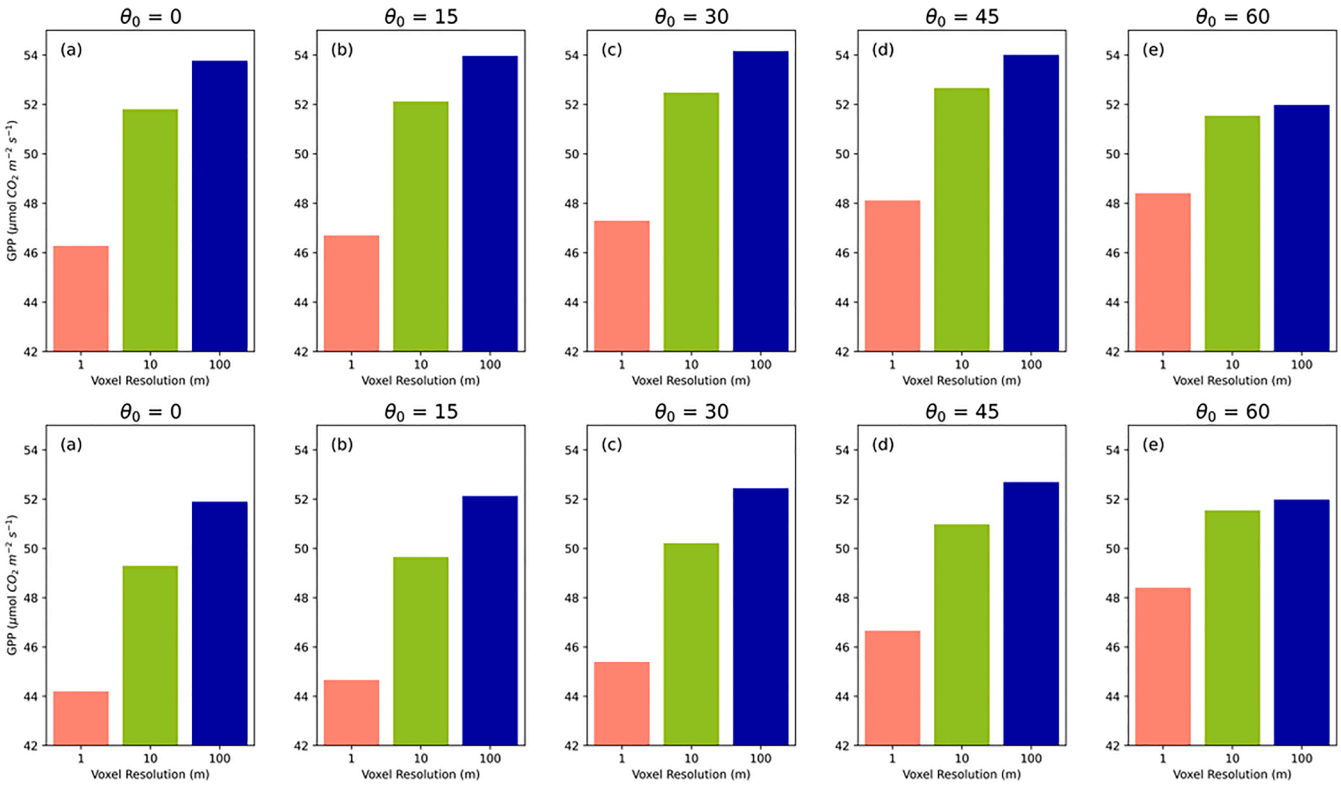

Fig. 12. The total canopy GPP for Wytham Woods at three resolutions (1 m, 10 m, 100 m, Fig. 1, Table 1), with both a spherical (top panels) and horizontal (lower panels) LAD prescribed, across five solar zenith angles, $\theta_0 = 0°$, 15°, 30°, 45°, 60°, with leaf temperature, $T_{Leaf} = 25$ °C and IPAR = 200 W m^{-2}.

canopy top, but not a value of zero at the canopy base. The coarsest resolution, where leaves are randomly distributed in the horizontal throughout the scene, leads to a profile that shows the largest GPP at the canopy top with an exponential decay. This result is analogous to the way photosynthesis is typically calculated in climate models. These profiles are a result of the different extinction profiles through the canopy as the LAI distribution changes – some profiles will start lower/higher in the canopy as the resolution of the input scene varies.

In the cases that we examined, making voxel sizes coarser, which we use as a proxy for decreasing structural detail in the calculation, increases the total canopy GPP. Some scenes show no variability with finer spatial resolution (e.g., Harvard), whereas others show a large variability (e.g., Maliau). These scenes that show more variability in GPP also have large horizontal variation of LAI is high, e.g., Wytham Woods and Maliau (Fig. 7). One notable result is the change in sensitivity to spatial resolution in Wytham after 20 m, which could suggest a change in processes captured, for example between crown-scale effects (e.g., 20 – 100 m) and branch scale (e.g., 1 – 2 m). This leads to a question of whether any other scenes would show similar effects if the TLS had been collected at an equally fine scale. Our results suggest that a lack of realistic vegetation structure in approaches currently used to describe radiation transfer in Earth system models will likely cause modelled GPP to be biased high. This is also probably masked by compensating biases elsewhere in the model, for example by adopting unrepresentative values of photosynthetic parameters such as V_{cmax} (Walker et al., 2017).

Within this work we have tested a wide range of environmental variables (temperature, solar zenith angle, incoming radiation, and diffuse fraction). We have also completed simulations testing whether the decrease in GPP with a finer structure holds when we vary canopy properties, such as LAI, LAD, and soil and leaf albedos. The findings are consistent across these sensitivity tests, that using a finer spatial resolution of canopy structure decreases GPP.

Clearly, incorporating high spatial resolution, 3D simulations of canopy radiative transfer into climate model calculations is not feasible, both from the perspective of computational expense and the need to find input data for forests globally. Consequently, some form of simplification or parameterisation is required. Traditionally this has been done using so-called clumping indices, which scale the LAI inside radiative transfer calculations to account for reduced interception of light due to self-organisation of leaves around stems and branches. This approach underlies the results of Braghiere et al. (2019), who used JULES, and Li et al. (2023) using CLM. In both studies, GPP was shown to increase almost everywhere on the land surface when clumping was introduced, and especially so in dense forests. The explanation provided is that additional light is transmitted through to shaded leaves lower in the canopy (in which photosynthesis tends to be light limited) and thus boosts GPP.

Our DART-modelled GPP has the same photosynthesis equations as JULES and so, in principle, could reproduce this effect. However, we show an almost ubiquitous decrease in GPP as finer structure is included in the simulations. A reason for this could be that the bulk effect of absorbing less light due to an increased number of gaps within the canopy could outweigh the additional photosynthesis by shaded leaves lower in the canopy suggested by previous work. However, we have made no comparison against the specific parameters (e.g., V_{cmax}) within these studies. Presently, our work suggests that simple clumping factors applied to two-stream canopy radiative transfer schemes may not be adequate tools to account for these effects in global simulations, especially in forests.

However, some areas of our study do differ to those previously conducted. One example is that as we have not utilised a full land surface model, we focus on instantaneous GPP, instead of temporally varying GPP (across a day, season, or a year). Further, Braghiere et al., (2019) and Li et al., (2023) focus on GPP at a global scale, and in this study we have only sampled six forest plots. It may be possible, by analysing additional plots, that we would find situation which supported the hypotheses presented in these papers.

More work is clearly needed to understand the full role of structure

and how to best incorporate it into existing Earth system model setups. In particular, this will require things such as finer resolution TLS (which may be complex within the field and require large amounts of person-time) across more sites covering a larger range of forest types, which can be processed to run multiple model types for model-intercomparisons. From this, data will need to be parameterised on large scales, e.g. using airborne or spaceborne lidar data. Then, data will need to be used as validation, requiring more field sites/towers and employing earth observation data. Additionally, more complex models that resolve better the forest canopy structure, e.g. SPARTACUS (Hogan et al., 2018), the two-stream model outlined in Pinty et al. (2006), and the modified two-stream model in Ni-Meisters et al. (2010).

5. Conclusions

We have introduced a methodology for calculation gross primary productivity from the DART model which follows a common approach used in the land surface schemes of Earth system models. We used this to explore the sensitivity of modelled GPP to assumptions about canopy structure inside Earth system models by creating DART scenes for six different forests using terrestrial lidar scanning data. We ran simulations at different spatial resolutions, which we used as a proxy for the amount of 3D structure we were accounting for. In almost all cases running the DART simulation at a finer spatial resolution resulted in a decrease in the modelled GPP. In the few cases where this did not happen, the increases in GPP were only marginal (< 2.5 %). This contrasts with several recent papers which show the opposite behaviour. We argue that the increases in GPP seen in these studies emerge because the turbid medium assumption cannot adequately account for the effect of clumping on photosynthesis. The sensitivity we observed exhibited across the six forests varied, with some showing little change in GPP with voxel resolution and others showing changes up to 25 %.

CRediT authorship contribution statement

Megan A. Stretton: Writing – review & editing, Writing – original draft, Visualization, Investigation, Formal analysis, Conceptualization. **Tristan Quaife:** Writing – review & editing, Supervision, Software, Project administration, Methodology, Funding acquisition, Conceptualization. **Phil Wilkes:** Writing – review & editing, Data curation. **Mat Disney:** Writing – review & editing, Data curation.

Declaration of competing interest

The authors declare that they have no known competing financial interests or personal relationships that could have appeared to influence the work reported in this paper.

Acknowledgements

This research was funded by UKRI NERC as part of the SPLICE project (NE/W006596/1). MD and PW acknowledge capital and travel funding from NERC National Centre for Earth Observation (NCEO), UCL; MD was funded in part via European Metrology Programme for Innovation and Research (EMPIR) award (ENV53 MetEOC-2).

Data availability

The DART simulation inputs and outputs, as well as the code used to compute photosynthesis from the DART output, analyse the model data, and create the figures is available at doi:10.5281/zenodo.10809422. In addition, this work requires the JULES Leaf Simulator, which is available at the UK Met Office code repository (https://code.metoffice.gov.uk/trac/utils/browser/leafsimulator/), released with no specific licence (registration required).The DART model is freely available for research at https://dart.omp.eu/.

Supplementary materials

Supplementary material associated with this article can be found, in the online version, at doi:10.1016/j.agrformet.2025.110437.

References

Alton, P., Mercado, L., North, P., 2006. A sensitivity analysis of the land-surface scheme JULES conducted for three forest biomes: biophysical parameters, model processes, and meteorological driving data. Global Biogeochem. Cycles 21. https://doi.org/10.1029/2005GB002653.

Baldocchi, D.D., Wilson, K.B., Gu, L., 2002. How the environment, canopy structure and canopy physiological functioning influence carbon, water and energy fluxes of a temperate broad-leaved deciduous forest - an assessment with the biophysical model CANOAK. Tree Physiol. https://doi.org/10.1093/treephys/22.15-16.1065.

Best, M.J., Pryor, M., Clark, D.B., Rooney, G.G., Essery, R..L.H., Ménard, C.B., Edwards, J.M., Hendry, M.A., Porson, A., Gedney, N., Mercado, L.M., Sitch, S., Blyth, E., Boucher, O., Cox, P.M., Grimmond, C.S.B., Harding, R.J., 2011. The joint UK land environment simulator (JULES), model description – Part 1: energy and water fluxes. Geosci. Model Dev 4, 677–699. https://doi.org/10.5194/GMD-4-677-2011.

Bonan, G.B., Patton, E.G., Harman, I.N., Oleson, K.W., Finnigan, J.J., Lu, Y., Burakowski, E.A., 2018. Modeling canopy-induced turbulence in the Earth system: A unified parameterization of turbulent exchange within plant canopies and the roughness sublayer (CLM-ml v0). Geosci. Model Dev. 11. https://doi.org/10.5194/gmd-11-1467-2018.

Braghiere, R.K., Quaife, T., Black, E., He, L., Chen, J.M., 2019. Underestimation of global photosynthesis in Earth system models due to representation of vegetation structure. Global Biogeochem. Cycles 33. https://doi.org/10.1029/2018GB006135.

Braghiere, R.K., Quaife, T., Black, E., Ryu, Y., Chen, Q., De Kauwe, M.G., Baldocchi, D., 2020. Influence of sun zenith angle on canopy clumping and the resulting impacts on photosynthesis. Agric. For. Meteorol. 291. https://doi.org/10.1016/j.agrformet.2020.108065.

Calders, K., Armston, J., Newnham, G., Herold, M., Goodwin, N., 2014. Implications of sensor configuration and topography on vertical plant profiles derived from terrestrial LiDAR. Agric. For. Meteorol. 194. https://doi.org/10.1016/j.agrformet.2014.03.022.

Calders, K., Origo, N., Burt, A., Disney, M., Nightingale, J., Raumonen, P., Åkerblom, M., Malhi, Y., Lewis, P., 2018. Realistic forest stand reconstruction from terrestrial LiDAR for radiative transfer modelling. Remote Sens. 10. https://doi.org/10.3390/rs10060933.

Chen, J.M., Mo, G., Pisek, J., Liu, J., Deng, F., Ishizawa, M., Chan, D., 2012. Effects of foliage clumping on the estimation of global terrestrial gross primary productivity. Global Biogeochem. Cycles 26. https://doi.org/10.1029/2010GB003996.

Chen, Y., Ryder, J., Bastrikov, V., McGrath, M.J., Naudts, K., Otto, J., Ottlé, C., Peylin, P., Polcher, J., Valade, A., Black, A., Elbers, J.A., Moors, E., Foken, T., Van Gorsel, E., Haverd, V., Heinesch, B., Tiedemann, F., Knohl, A., Launiainen, S., Loustau, D., Ogeé, J., Vessala, T., Luyssaert, S., 2016. Evaluating the performance of land surface model ORCHIDEE-CAN v1.0 on water and energy flux estimation with a single-and multi-layer energy budget scheme. Geosci. Model Dev. 9. https://doi.org/10.5194/gmd-9-2951-2016.

Ciais, P., Sabine, C., Bala, G., Bopp, L., Brovkin, V., Canadell, J., Chhabra, A., DeFries, R., Galloway, J., Heimann, M., Jones, C., Quéré, C. Le, Myneni, R.B., Piao, S., Thornton, P., 2013. Carbon and other biogeochemical cycles. In: Climate Change 2013: the physical science Basis., Climate Change 2013 - the physical science Basis.

Clark, D.B., Mercado, L.M., Sitch, S., Jones, C.D., Gedney, N., Best, M.J., Pryor, M., Rooney, G.G., Essery, R.L.H., Blyth, E., Boucher, O., Harding, R.J., Huntingford, C., Cox, P.M., 2011. The Joint UK Land Environment Simulator (JULES), model description – Part 2: carbon fluxes and vegetation dynamics. Geosci. Model Dev 4, 701–722. https://doi.org/10.5194/GMD-4-701-2011.

Collatz, G., Ribas-Carbo, M., Berry, J., 1992. Coupled photosynthesis-stomatal conductance model for leaves of C4 plants. Funct. Plant Biol. 19. https://doi.org/10.1071/pp9920519.

Collatz, G.J., Ball, J.T., Grivet, C., Berry, J.A., 1991. Physiological and environmental regulation of stomatal conductance, photosynthesis and transpiration: a model that includes a laminar boundary layer. Agric. For. Meteorol. 54. https://doi.org/10.1016/0168-1923(91)90002-8.

Dai, Y., Dickinson, R.E., Wang, Y.P., 2004. A two-big-leaf model for canopy temperature, photosynthesis, and stomatal conductance. J. Clim. 17. https://doi.org/10.1175/1520-0442(2004)017<2281:ATMFCT>2.0.CO;2.

De Boissieu, F., Heuschmidt, F., Lauret, N., Ebengo, D.M., Vincent, G., Feret, J.B., Yin, T., Gastellu-Etchegorry, J.P., Costeraste, J., Lefevre-Fonollosa, M.J., Durrieu, S., 2023. Validation of the DART model for airborne laser scanner simulations on complex forest environments. IEEE J. Sel. Top. Appl. Earth Obs. Remote Sens. 16, 8379–8394. https://doi.org/10.1109/JSTARS.2023.3302030.

Demarez, V., Gastellu-Etchegorry, J.P., Mordelet, P., Tosca, C., Marty, G., Guillevic, P., 2000. Modeling of the radiation regime and photosynthesis of a finite canopy using the DART model. Influence of canopy architecture assumptions and border effects. Agronomie 20. https://doi.org/10.1051/agro:2000125.

Dickinson, R.E., 1983. Land surface processes and climate—Surface albedos and energy balance. Adv. Geophys. 25. https://doi.org/10.1016/S0065-2687(08)60176-4.

Dickinson, R.E., Oleson, K.W., Bonan, G., Hoffman, F., Thornton, P., Vertenstein, M., Yang, Z.L., Zeng, X., 2006. The community land model and its climate statistics as a

component of the community climate system model. J. Clim. 19, 2302–2324. https://doi.org/10.1175/JCLI3742.1.
Fisher, R.A., Muszala, S., Verteinstein, M., Lawrence, P., Xu, C., McDowell, N.G., Knox, R. G., Koven, C., Holm, J., Rogers, B.M., Spessa, A., Lawrence, D., Bonan, G., 2015. Taking off the training wheels: the properties of a dynamic vegetation model without climate envelopes, CLM4.5(ED). Geosci. Model Dev 8. https://doi.org/10.5194/gmd-8-3593-2015.
Friedlingstein, P., O'Sullivan, M., Jones, M.W., Andrew, R.M., Hauck, J., Olsen, A., Peters, G.P., Peters, W., Pongratz, J., Sitch, S., Le Quéré, C., Canadell, J.G., Ciais, P., Jackson, R.B., Alin, S., Aragão, L.E.O.C., Arneth, A., Arora, V., Bates, N.R., Becker, M., Benoit-Cattin, A., Bittig, H.C., Bopp, L., Bultan, S., Chandra, N., Chevallier, F., Chini, L.P., Evans, W., Florentie, L., Forster, P.M., Gasser, T., Gehlen, M., Gilfillan, D., Gkritzalis, T., Gregor, L., Gruber, N., Harris, I., Hartung, K., Haverd, V., Houghton, R.A., Ilyina, T., Jain, A.K., Joetzjer, E., Kadono, K., Kato, E., Kitidis, V., Korsbakken, J.I., Landschützer, P., Lefèvre, N., Lenton, A., Lienert, S., Liu, Z., Lombardozzi, D., Marland, G., Metzl, N., Munro, D.R., Nabel, J.E.M.S., Nakaoka, S.I., Niwa, Y., O'Brien, K., Ono, T., Palmer, P.I., Pierrot, D., Poulter, B., Resplandy, L., Robertson, E., Rödenbeck, C., Schwinger, J., Séférian, R., Skjelvan, I., Smith, A.J.P., Sutton, A.J., Tanhua, T., Tans, P.P., Tian, H., Tilbrook, B., Van Der Werf, G., Vuichard, N., Walker, A.P., Wanninkhof, R., Watson, A.J., Willis, D., Wiltshire, A.J., Yuan, W., Yue, X., Zaehle, S., 2020. Global carbon budget 2020. Earth Syst. Sci. Data 12. https://doi.org/10.5194/essd-12-3269-2020.
Gastellu-Etchegorry, J.P., Yin, T., Lauret, N., Cajgfinger, T., Gregoire, T., Grau, E., Feret, J.B., Lopes, M., Guilleux, J., Dedieu, G., Malenovskỳ, Z., Cook, B.D., Morton, D., Rubio, J., Durrieu, S., Cazanave, G., Martin, E., Ristorcelli, T., 2015. Discrete anisotropic radiative transfer (DART 5) for modeling airborne and satellite spectroradiometer and LIDAR acquisitions of natural and urban landscapes. Remote Sens 7, 1667–1701. https://doi.org/10.3390/rs70201667.
He, L., Chen, J.M., Pisek, J., Schaaf, C.B., Strahler, A.H., 2012. Global clumping index map derived from the MODIS BRDF product. Remote Sens. Environ. 119. https://doi.org/10.1016/j.rse.2011.12.008.
Hogan, R.J., Quaife, T., Braghiere, R., 2018. Fast matrix treatment of 3-D radiative transfer in vegetation canopies: SPARTACUS-vegetation 1.1. Geosci. Model dev. 11, 339–350. https://doi.org/10.5194/gmd-11-339-2018.
Janoutová, R., Homolová, L., Malenovskỳ, Z., Hanuš, J., Lauret, N., Gastellu-Etchegorry, J.P., 2019. Influence of 3D spruce tree representation on accuracy of airborne and satellite forest reflectance simulated in DART. Forests 10. https://doi.org/10.3390/f10030292.
Jupp, D.L.B., Lovell, J.L., 2007. Airborne and ground-based lidar systems for forest measurement : background and principles. Atmos. Res.
Kattge, J., Knorr, W., Raddatz, T., Wirth, C., 2009. Quantifying photosynthetic capacity and its relationship to leaf nitrogen content for global-scale terrestrial biosphere models. Glob. Chang. Biol. 15. https://doi.org/10.1111/j.1365-2486.2008.01744.x.
Kobayashi, H., Iwabuchi, H., 2008. A coupled 1-D atmosphere and 3-D canopy radiative transfer model for canopy reflectance, light environment, and photosynthesis simulation in a heterogeneous landscape. Remote Sens. Environ. 112, 173–185. https://doi.org/10.1016/J.RSE.2007.04.010.
Kucharik, C.J., Norman, J.M., Gower, S.T., 1999. Characterization of radiation regimes in nonrandom forest canopies: theory, measurements, and a simplified modeling approach. Tree Physiol. 19. https://doi.org/10.1093/treephys/19.11.695.
Le Quéré, C., Andrew, R.M., Friedlingstein, P., Sitch, S., Hauck, J., Pongratz, J., Pickers, P.A., Korsbakken, J.I., Peters, G.P., Canadell, J.G., Arneth, A., Arora, V.K., Barbero, L., Bastos, A., Bopp, L., Chevallier, F., Chini, L.P., Ciais, P., Doney, S.C., Gkritzalis, T., Goll, D.S., Harris, I., Haverd, V., Hoffman, F.M., Hoppema, M., Houghton, R.A., Hurtt, G., Ilyina, T., Jain, A.K., Johannessen, T., Jones, C.D., Kato, E., Keeling, R.F., Klein Goldewijk, K., Landschützer, P., Lefèvre, N., Lienert, S., Liu, Z., Lombardozzi, D., Metzl, N., Munro, D.R., Nabel, J.E.M.S., Nakaoka, S.-I., Neill, C., Olsen, A., Ono, T., Patra, P., Peregon, A., Peters, W., Peylin, P., Pfeil, B., Pierrot, D., Poulter, B., Rehder, G., Resplandy, L., Robertson, E., Rocher, M., Rödenbeck, C., Schuster, U., Schwinger, J., Séférian, R., Skjelvan, I., Steinhoff, T., Sutton, A., Tans, P.P., Tian, H., Tilbrook, B., Tubiello, F.N., Van Der Laan-Luijkx, I.T., Van Der Werf, G.R., Viovy, N., Walker, A.P., Wiltshire, A.J., Wright, R., Zaehle, S., Zheng, B., 2018. Global Carbon Budget 2018. Earth Syst. Sci. Data 10, 2141–2194. https://doi.org/10.5194/essd-10-2141-2018.
Li, F., Hao, D., Zhu, Q., Yuan, K., Braghiere, R.K., He, L., Luo, X., Wei, S., Riley, W.J., Zeng, Y., Chen, M., 2023. Vegetation clumping modulates global photosynthesis through adjusting canopy light environment. Glob. Chang. Biol. 29. https://doi.org/10.1111/gcb.16503.
Liu, C., Calders, K., Meunier, F., Gastellu-Etchegorry, J.P., Nightingale, J., Disney, M., Origo, N., Woodgate, W., Verbeeck, H., 2022. Implications of 3D forest stand reconstruction methods for radiative transfer modeling: A case study in the temperate deciduous forest. J. Geophys. Res. Atmos. 127. https://doi.org/10.1029/2021JD036175.
Loew, A., Van Bodegom, P.M., Widlowski, J.L., Otto, J., Quaife, T., Pinty, B., Raddatz, T., 2014. Do we (need to) care about canopy radiation schemes in DGVMs? Caveats and potential impacts. Biogeosciences 11. https://doi.org/10.5194/bg-11-1873-2014.
Longo, M., Knox, R.G., Medvigy, D.M., Levine, N.M., Dietze, M.C., Kim, Y., Swann, A.L.S., Zhang, K., Rollinson, C.R., Bras, R.L., Wofsy, S.C., Moorcroft, P.R., 2019. The biophysics, ecology, and biogeochemistry of functionally diverse, vertically and horizontally heterogeneous ecosystems: The ecosystem demography model, version 2.2-part 1: model description. Geosci. Model Dev. 12. https://doi.org/10.5194/gmd-12-4309-2019.
Madani, N., Kimball, J.S., Ballantyne, A.P., Affleck, D.L.R., Van Bodegom, P.M., Reich, P. B., Kattge, J., Sala, A., Nazeri, M., Jones, M.O., Zhao, M., Running, S.W., 2018. Future global productivity will be affected by plant trait response to climate. Sci. Rep. 8. https://doi.org/10.1038/s41598-018-21172-9.
Malenovský, Z., Regaieg, O., Yin, T., Lauret, N., Guilleux, J., Chavanon, E., Duran, N., Janoutová, R., Delavois, A., Meynier, J., Medjdoub, G., Yang, P., van der Tol, C., Morton, D., Cook, B.D., Gastellu-Etchegorry, J.P., 2021. Discrete anisotropic radiative transfer modelling of solar-induced chlorophyll fluorescence: structural impacts in geometrically explicit vegetation canopies. Remote Sens. Environ 263. https://doi.org/10.1016/j.rse.2021.112564.
Mercado, L.M., Bellouin, N., Sitch, S., Boucher, O., Huntingford, C., Wild, M., Cox, P.M., 2009. Impact of changes in diffuse radiation on the global land carbon sink. Nat 1014–1017. https://doi.org/10.1038/nature07949, 2009 4587241 458.
Ni-Meister, W., Yang, W., Kiang, N.Y., 2010. A clumped-foliage canopy radiative transfer model for a global dynamic terrestrial ecosystem model. I: theory. Agric. For. Meteorol. 150. https://doi.org/10.1016/j.agrformet.2010.02.009.
Nilson, T., 1971. A theoretical analysis of the frequency of gaps in plant stands. Agric. Meteorol. 8. https://doi.org/10.1016/0002-1571(71)90092-6.
Norman, J.M., 1993. Scaling processes between leaf and canopy levels. Scaling Physiological Processes. https://doi.org/10.1016/b978-0-12-233440-5.50010-5.
Peaucelle, M., Bacour, C., Ciais, P., Vuichard, N., Kuppel, S., Peñuelas, J., Belelli Marchesini, L., Blanken, P.D., Buchmann, N., Chen, J., Delpierre, N., Desai, A.R., Dufrene, E., Gianelle, D., Gimeno-Colera, C., Gruening, C., Helfter, C., Hörtnagl, L., Ibrom, A., Joffre, R., Kato, T., Kolb, T.E., Law, B., Lindroth, A., Mammarella, I., Merbold, L., Minerbi, S., Montagnani, L., Šigut, L., Sutton, M., Varlagin, A., Vesala, T., Wohlfahrt, G., Wolf, S., Yakir, D., Viovy, N., 2019. Covariations between plant functional traits emerge from constraining parameterization of a terrestrial biosphere model. Glob. Ecol. Biogeogr. 28. https://doi.org/10.1111/geb.12937.
Pinty, B., Lavergne, T., Dickinson, R.E., Widlowski, J.L., Gobron, N., Verstraete, M.M., 2006. Simplifying the interaction of land surfaces with radiation for relating remote sensing products to climate models. J. Geophys. Res. Atmos. 111. https://doi.org/10.1029/2005JD005952.
Pinty, B., Widlowski, J.L., Taberner, M., Gobron, N., Verstraete, M.M., Disney, M., Gascon, F., Gastellu, J.P., Jiang, L., Kuusk, A., Lewis, P., Li, X., Ni-Meister, W., Nilson, T., North, P., Qin, W., Su, L., Tang, S., Thompson, R., Verhoef, W., Wang, H., Wang, J., Yan, G., Zang, H., 2004. Radiation transfer model intercomparison (RAMI) exercise: results from the second phase. J. Geophys. Res. D Atmos. https://doi.org/10.1029/2003jd004252.
Regaieg, O., Lauret, N., Wang, Y., Guilleux, J., Chavanon, E., Gastellu-Etchegorry, J.P., 2023. Bi-directional Monte-Carlo modelling of solar-induced chlorophyll fluorescence images for 3D vegetation canopies in the DART model. Int. J. Appl. Earth Obs. Geoinf. 118, 103254. https://doi.org/10.1016/J.JAG.2023.103254.
Revilla, S., Lamelas, M.T., Domingo, D., de la Riva, J., Montorio, R., Montealegre, A.L., García-Martín, A., 2021. Assessing the potential of the DART model to discrete return LiDAR simulation—Application to fuel type mapping. Remote Sens 13, 342. https://doi.org/10.3390/RS13030342, 2021Page13, 342.
Rewald, B., Pena, R., Liu, C., Li, Y., Yan, P., He, N., 2021. How to improve the predictions of plant functional traits on ecosystem functioning? Front. Plant Sci. 12, 622260. https://doi.org/10.3389/fpls.2021.622260. |. www.frontiersin.org.
Ryder, J., Polcher, J., Peylin, P., Ottlé, C., Chen, Y., Van Gorsel, E., Haverd, V., McGrath, M.J., Naudts, K., Otto, J., Valade, A., Luyssaert, S., 2016. A multi-layer land surface energy budget model for implicit coupling with global atmospheric simulations. Geosci. Model Dev. 9. https://doi.org/10.5194/gmd-9-223-2016.
Sellers, P.J., 1985. Canopy reflectance, photosynthesis and transpiration. Int. J. Remote Sens. 6. https://doi.org/10.1080/01431168508948283.
Shiklomanov, A.N., Dietze, M.C., Fer, I., Viskari, T., Serbin, S.P., 2021. Cutting out the middleman: calibrating and validating a dynamic vegetation model (ED2-PROSPECT5) using remotely sensed surface reflectance. Geosci. Model Dev. 14. https://doi.org/10.5194/gmd-14-2603-2021.
Sinclair, T.R., Murphy, C.E., Knoerr, K.R., 1976. Development and evaluation of simplified models for simulating canopy photosynthesis and transpiration. J. Appl. Ecol. 13, 813. https://doi.org/10.2307/2402257.
Sitch, S., Huntingford, C., Gedney, N., Levy, P.E., Lomas, M., Piao, S.L., Betts, R., Ciais, P., Cox, P., Friedlingstein, P., Jones, C.D., Prentice, I.C., Woodward, F.I., 2008. Evaluation of the terrestrial carbon cycle, future plant geography and climate-carbon cycle feedbacks using five dynamic Global Vegetation models (DGVMs). Glob. Chang. Biol. 14. https://doi.org/10.1111/j.1365-2486.2008.01626.x.
Sokolov, A.P., Kicklighter, D.W., Melillo, J.M., Felzer, B.S., Schlosser, C.A., Cronin, T.W., 2008. Consequences of considering carbon–Nitrogen interactions on the feedbacks between climate and the terrestrial carbon cycle. J. Clim. 21, 3776–3796. https://doi.org/10.1175/2008JCLI2038.1.
Song, J., Miller, G.R., Cahill, A.T., Aparecido, L.M.T., Moore, G.W., 2021. Modeling profiles of micrometeorological variables in a tropical premontane rainforest using multi-layered CLM (CLM-ML). J. Adv. Model. Earth Syst. 13. https://doi.org/10.1029/2020MS002259.
Sprintsin, M., Chen, J.M., Desai, A., Gough, C.M., 2012. Evaluation of leaf-to-canopy upscaling methodologies against carbon flux data in North America. J. Geophys. Res. Biogeosciences 117. https://doi.org/10.1029/2010JG001407.
Thornton, P.E., Lamarque, J.F., Rosenbloom, N.A., Mahowald, N.M., 2007. Influence of carbon-nitrogen cycle coupling on land model response to CO2 fertilization and climate variability. Global Biogeochem. Cycles 21, 4018. https://doi.org/10.1029/2006GB002868.
Walker, A.P., Quaife, T., van Bodegom, P.M., De Kauwe, M.G., Keenan, T.F., Joiner, J., Lomas, M.R., MacBean, N., Xu, C., Yang, X., Woodward, F.I., 2017. The impact of alternative trait-scaling hypotheses for the maximum photosynthetic carboxylation rate (Vcmax) on global gross primary production. New. Phytol. 215. https://doi.org/10.1111/nph.14623.
Widlowski, J.L., Mio, C., Disney, M., Adams, J., Andredakis, I., Atzberger, C., Brennan, J., Busetto, L., Chelle, M., Ceccherini, G., Colombo, R., Côté, J.F., Eenmäe, A., Essery, R., Gastellu-Etchegorry, J.P., Gobron, N., Grau, E., Haverd, V., Homolová, L.,

Huang, H., Hunt, L., Kobayashi, H., Koetz, B., Kuusk, A., Kuusk, J., Lang, M., Lewis, P.E., Lovell, J.L., Malenovský, Z., Meroni, M., Morsdorf, F., Mõttus, M., Ni-Meister, W., Pinty, B., Rautiainen, M., Schlerf, M., Somers, B., Stuckens, J., Verstraete, M.M., Yang, W., Zhao, F., Zenone, T., 2015. The fourth phase of the radiative transfer model intercomparison (RAMI) exercise: actual canopy scenarios and conformity testing. Remote Sens. Environ. https://doi.org/10.1016/j.rse.2015.08.016.

Widlowski, J.L., Taberner, M., Pinty, B., Bruniquel-Pinel, V., Disney, M., Fernandes, R., Gastellu-Etchegorry, J.P., Gobron, N., Kuusk, A., Lavergne, T., Leblanc, S., Lewis, P. E., Martin, E., Mõttus, M., North, P.R.J., Qin, W., Robustelli, M., Rochdi, N., Ruiloba, R., Soler, C., Thompson, R., Verhoef, W., Verstraete, M.M., Xie, D., 2007. Third radiation transfer model intercomparison (RAMI) exercise: documenting progress in canopy reflectance models. J. Geophys. Res. Atmos. https://doi.org/10.1029/2006JD007821.

Wilkes, P., Lau, A., Disney, M., Calders, K., Burt, A., Gonzalez de Tanago, J., Bartholomeus, H., Brede, B., Herold, M., 2017. Data acquisition considerations for terrestrial laser scanning of forest plots. Remote Sens. Environ. 196. https://doi.org/10.1016/j.rse.2017.04.030.

Yan, P., He, N., Yu, K., Xu, L., Van Meerbeek, K., 2023. Integrating multiple plant functional traits to predict ecosystem productivity. Commun. Biol. 6. https://doi.org/10.1038/s42003-023-04626-3.